

# INTENSITY-FIELD CORRELATIONS OF NON-CLASSICAL LIGHT

H. J. CARMICHAEL  
*Department of Physics*  
*University of Auckland*  
*Private Bag 92019*  
*Auckland, 1301, New Zealand.*

G. T. FOSTER  
*Department of Physics and Astronomy*  
*Hunter College, CUNY*  
*New York, NY 10021, United States*

L. A. OROZCO, J. E. REINER  
*Department of Physics and Astronomy*  
*State University of New York*  
*Stony Brook NY 11794-3800, United States*

AND

P. R. RICE  
*Department of Physics*  
*Miami University*  
*Oxford, OH 45056, United States*

**Abstract.** The intensity-field correlation function of the electromagnetic field is a tool for studying the quantum fluctuations of light. This review introduces the correlation function and its relationship to quadrature squeezing, develops conditions (Schwartz inequalities) to distinguish between nonclassical and classical field fluctuations, and discusses its connection to weak measurements. The theoretical ideas are illustrated by calculations for three sample systems: the optical parametric oscillator, a cavity QED system, and the composite system of a single atom coupled to an optical parametric oscillator. The results of experimental measurements on a cavity QED system are also reviewed.



## Table of Contents

<b>1</b>	<b>INTENSITY-FIELD CORRELATIONS OF NON-CLASSICAL LIGHT</b>	<b>1</b>
1	Introduction . . . . .	4
2	Theory . . . . .	6
2.1	The Intensity-Field Correlation Function $h_\theta(\tau)$ . . .	6
2.2	Classical Bounds for $h_\theta(\tau)$ . . . . .	10
2.3	Time Reversal Properties of $h_\theta(\tau)$ . . . . .	11
2.4	Intensity-Field Correlations in Classical Optics . . .	12
3	Examples . . . . .	13
3.1	Optical Parametric Oscillator . . . . .	16
3.2	Cavity QED . . . . .	18
3.3	Two-Level Atom in an Optical Parametric Oscillator	28
4	Experiment in Cavity QED . . . . .	32
4.1	Cavity QED Apparatus . . . . .	33
4.2	Conditional Homodyne Detector . . . . .	34
4.3	Measurements . . . . .	36
5	Equal-Time Cross- and Auto-Correlations . . . . .	41
5.1	Cross-Correlations . . . . .	42
6	Quantum Measurements and Quantum Feedback . . . . .	45
6.1	Weak Measurements . . . . .	45
6.2	Vacuum State Squeezing Versus Squeezed Classical Noise . . . . .	46
6.3	Application of $h_\theta(\tau)$ to Quantum Feedback . . . . .	47
7	Conclusion and Outlook . . . . .	50

## 1. Introduction

Studies of the fluctuations of light have occupied quantum optics since its beginnings. Experimental work in the field has followed two broad lines, the first focused on intensity fluctuations and the measurement of correlations between pairs of photon detections [particle aspect of light] (BROWN AND TWISS (1956), KIMBLE, DAGENAIS AND MANDEL (1977)), and the second primarily concerned with squeezing experiments where the fluctuation variance of a quadrature amplitude of the optical field is measured [wave aspect of light] (SLUSHER, HOLLBERG, MERTZ, YURKE AND VALLEY (1985), LOUDON AND KNIGHT (1987), KIMBLE AND WALLS (1987)).

Until recently, these two lines of investigation remained separate. It is now possible, however, to combine them in a new approach that detects the fluctuations of an electromagnetic field by correlating its intensity and amplitude (CARMICHAEL, CASTRO-BELTRAN, FOSTER AND OROZCO (2000), FOSTER, OROZCO, CASTRO-BELTRAN AND CARMICHAEL (2000*a*)). The approach draws the particle and wave aspects of light together, and opens up a third-order correlation function of the electromagnetic field to experimental study. The new measurement strategy builds upon the relationship between quantum optical correlation functions and conditional measurements (MANDEL AND WOLF (1995)), and its physical interpretation is therefore illuminated through quantum trajectory calculations (CARMICHAEL (1993*a*)).

Historically, it was the development of the intensity-intensity correlation technique of Hanbury Brown and Twiss (HBT) (BROWN AND TWISS (1956)) that provided the stimulus for a systematic treatment of optical coherence within the framework of quantum mechanics (GLAUBER (1963*a*), GLAUBER (1963*b*), GLAUBER (1963*c*)). A notable feature of the HBT approach is its reliance on a *conditional* measurement—i.e., data is collected on the cue of a conditioning photon count that identifies those times when an intensity fluctuation is in progress. In this way, the average fluctuation is recovered as a conditional evolution over time, and a sensitive probe of the nonclassicality of light is obtained.

The standard squeezing measurement is not, by way of contrast, a conditional measurement. Through balanced homodyne detection (YUEN AND CHAN (1983*a*), YUEN AND CHAN (1983*b*)), it effectively measures the sub-Poissonian variance of a photon counting distribution, after the photon counts have been integrated over many correlation times. The measurement is insensitive to fluctuations at low photon flux and the observed degree of squeezing is degraded by collection and detection inefficiencies. The measurement is resolved in the frequency domain and does not recover an evolution of the fluctuations over time.

The intensity-field correlation function is measured through the *conditional* detection of the quadrature amplitude fluctuations of light. The measurement cross-correlates the photocurrent of a balanced homodyne detector (BHD) with an initiating photon count in a natural extension of the HBT technique. It is extremely sensitive to the nonclassicality of light at low photon flux (weakly squeezed light) and, given sufficient detection bandwidth, resolves the fluctuations in time. For the case of Gaussian statistics, CARMICHAEL, CASTRO-BELTRAN, FOSTER AND OROZCO (2000) showed that the full spectrum of squeezing is recovered from the Fourier transform of the time-resolved fluctuation. The measurement, like the HBT technique, is independent of detection efficiency, except for the inevitable efficiency-dependence in the signal-to-noise ratio.

To date, intensity-field correlations have been explored for the optical parametric oscillator (OPO) (CARMICHAEL, CASTRO-BELTRAN, FOSTER AND OROZCO (2000)), in both theoretical (CARMICHAEL, CASTRO-BELTRAN, FOSTER AND OROZCO (2000), REINER, SMITH, OROZCO, CARMICHAEL AND RICE (2001)) and experimental (FOSTER, OROZCO, CASTRO-BELTRAN AND CARMICHAEL (2000*a*), FOSTER, SMITH, REINER AND OROZCO (2002)) studies of cavity QED, and for a single two-level atom coupled to an OPO (STRIMBU AND RICE (2003)). On the theoretical side, connections have been made to fundamental questions in quantum measurement theory and statistical physics. WISEMAN (2002), for example, has demonstrated a connection with weak measurements. CARMICHAEL (2003) has shown that, in contrast to a conventional squeezing measurement, conditional homodyne detection distinguishes *qualitatively* between vacuum state squeezing and squeezed classical noise. DENISOV, CASTRO-BELTRAN AND CARMICHAEL (2002) explored the time-reversal properties of the intensity-field correlations. They show that while the intensity-intensity correlation function is necessarily time symmetric, the intensity-field correlation function may be time asymmetric for non-Gaussian fluctuations. The time asymmetry indicates a breakdown of detailed balance.

In related but earlier work, YURKE AND STOLER (1987) proposed using intensity-field correlations between signal and idler channels to prepare and observe Fock states in the process of parametric down conversion. Recently, the tomographic reconstruction of a one-photon state was achieved working with an extension of their technique (CRISPINO, GIUSEPPE, MARTINI, MATALONI AND KANATOULIS (2000), LVOVSKY, HANSEN, AICHELE, BENSON, MLYNEK AND SCHILLER (2001)). The reconstruction relies on a time-integrated correlation, since the time scales in parametric down conversion are too short for current technology to follow the fluctuation over time. Intensity-field correlations also arise, more indirectly, in various other contexts: VYAS AND SINGH (2000), DENG, ERENDO, VYAS AND SINGH

(2001) on the degenerate OPO and VOGEL (1991) for resonance fluorescence.

The review is organized as follows. We begin, in Sec. 2, by presenting the general theoretical framework for the measurement of intensity-field correlations, including a discussion of the time-reversal properties of the correlation function. Section 3 illustrates the ideas with theoretical calculations for three specific quantum optical systems. The results of experiments in cavity QED are then presented in Sec. 4; there we give a thorough description of the experimental apparatus required. In Sec. 5 we review work on time-integrated intensity-field correlations in parametric down conversion. We finish, in Sec. 6, with an overview of the impact intensity-field correlations have made in the area of quantum measurement theory.

## 2. Theory

Figure 1 shows a schematic of the intensity-field correlator. It is based upon the HBT intensity correlator implemented in the modern “start”/“stop” scheme found for example in FOSTER, MIELKE AND OROZCO (2000*b*). The principal difference is that there is a balanced homodyne detector (BHD) in place of the second photon detector in what would normally be the “stop” channel; so it is appropriate to name this method as conditional homodyne detection (CHD). Operation of the correlator proceeds as follows: within a few correlation times before and after each “start”, the homodyne current  $I(t)$  is digitized, recorded, and used to update a cumulative average; averaging  $N_s$  such samples reduces the shot noise so that the surviving signal is a conditional average of the quadrature amplitude fluctuations of the input optical field.

### 2.1. THE INTENSITY-FIELD CORRELATION FUNCTION $H_\theta(\tau)$

For a more detailed analysis of the measurement, we consider a general optical source with power bandwidth  $2\kappa$  and output source-field  $\sqrt{2\kappa}\hat{b}$  (in units of the square-root of photon flux). In order to record a nonzero signal, the firing of the “start” detector must be biased towards the identification of quadrature amplitude fluctuations of a particular sign. To achieve this, a coherent offset of the source-field is generally needed (BS1 in Fig. 1). The offset also carries an adjustable phase, allowing the free selection of the quadrature to be measured. The input field to the correlator is then expressed in terms of the source field as

$$\sqrt{2\kappa}\hat{a} = \sqrt{2\kappa}(\hat{b} + Ae^{i\vartheta}), \quad (1)$$

where  $Ae^{i\vartheta}$  is determined by the complex amplitude of the offset. [A similar offset is used in some quantum state reconstruction schemes (BANASZEK

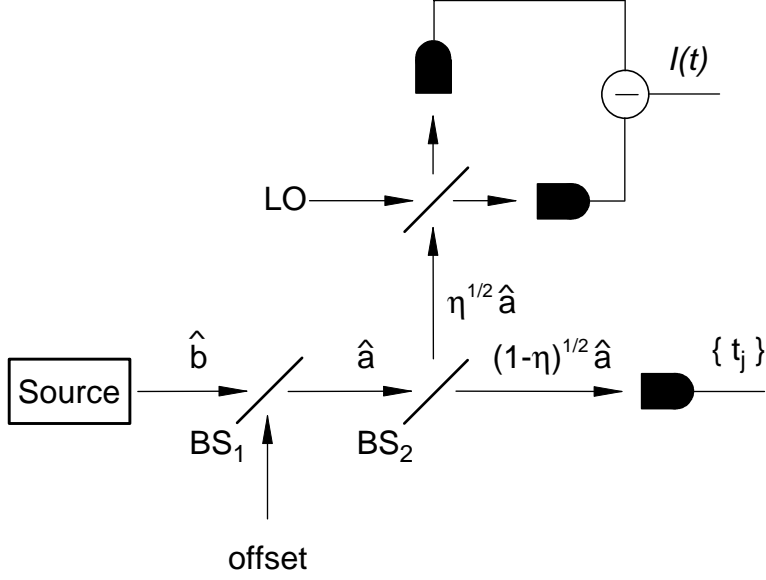


Figure 1. Schematic of the intensity-field correlator. The homodyne current  $I(t)$  is sampled over a series of time windows,  $t_j - \tau_{\max} \leq t \leq t_j + \tau_{\max}$ , each centered on a “start” time  $t_j$ .

AND WÓDKIEWICZ (1996), WALLENTOWITZ AND VOGEL (1996), LUTTERBACK AND DAVIDOVICH (1997)]. Sometimes the source-field has a non-zero mean amplitude, as is the case for the cavity QED system considered in Sec. 4. In such a case, the offset is not needed.

A fraction  $\eta$  of the input light is now sent to the balanced homodyne detector, with the remaining fraction  $1 - \eta$  going to the photon detector in the “start” channel (BS2 in Fig. 1). The photon flux operator at the photon detector is thus given in terms of the photon number operator for the source field (for simplicity, free-field operators are neglected as they do not contribute to normal-ordered averages):

$$\hat{S} = (1 - \eta)2\kappa\hat{a}^\dagger\hat{a}. \quad (2)$$

The balanced homodyne detector samples the quadrature phase amplitude that is in phase with the local oscillator field (LO in Fig. 1), with operator value

$$\hat{D} = 2\sqrt{\eta 2\kappa}\hat{a}_\theta, \quad \hat{a}_\theta \equiv \frac{1}{2}[\hat{a}e^{-i\theta} + \hat{a}^\dagger e^{i\theta}], \quad (3)$$

where  $\theta$  is the LO phase. The conditional homodyne photocurrent, averaged over the  $N_s$  “starts”, is then

$$H_\theta(\tau) = \frac{\langle : \hat{S}(t)\hat{D}(t+\tau) : \rangle}{\langle \hat{S} \rangle} + \xi(\tau); \quad (4)$$

$\langle : : \rangle$  denotes time and normal ordering, and  $\xi(t)$  is the residual local oscillator shot noise that is present because the ensemble average is taken over a finite number of samples only; its magnitude depends in the usual way on detection bandwidth and the number of samples  $N_s$ .

For positive  $\tau$ ,  $H_\theta(\tau)$  can be factorized in a straightforward way with the help of the quantum regression formula to give

$$H_\theta(\tau) = \langle \hat{D}(\tau, \theta) \rangle_c + \xi(\tau), \quad (5)$$

where the subscript  $c$  denotes conditioning of the state at time  $t$  on the detection of a photon. This is one of the most powerful results of the intensity-field correlation function in its quantum mechanical formulation; it gives access to the conditional dynamics of the quadrature phase amplitudes of the field, similar to the manner in which the intensity-intensity correlation function gives the conditional dynamics of the intensity (CARMICHAEL, BRECHA AND RICE (1991), BRECHA, RICE AND XIAO (1999)). For negative  $\tau$ , a construction of the post-selected conditional dynamics may be made on the basis of Bayesian inference (Sec. 6.1).

When the source field is small and non-classical, its fluctuations, a manifestation of the uncertainty principle, dominate over its steady-state amplitude. It is these fluctuations that are of interest, and therefore the input-field operator  $\hat{a}$  is conveniently decomposed as  $\hat{a} = \alpha + \Delta\hat{a}$ , with  $\alpha = \langle \hat{a} \rangle = |\alpha|e^{i\phi}$ , and  $\Delta\hat{a} = \Delta\hat{b} \equiv \hat{b} - \langle \hat{b} \rangle$  the fluctuation of interest. We now substitute Eqs. (2) and (3) into Eq. (4), and at the same time make the decomposition into a mean field plus fluctuation. In addition, for the present discussion we make the assumption, clearly valid for the case of Gaussian statistics, that third order moments of the field fluctuations vanish. The resulting correlation function in terms of the quadrature fluctuation  $\Delta\hat{a}_\phi = (\Delta\hat{a}e^{-i\phi} + \Delta\hat{a}^\dagger e^{i\phi})/2$  is:

$$H_{\theta,\phi}(\tau) = \sqrt{\eta 2\kappa} 2|\alpha| \left( \cos(\phi - \theta) + \frac{2\langle : \Delta\hat{a}_\phi(0)\Delta\hat{a}_\theta(\tau) : \rangle}{|\alpha|^2 + \langle \Delta\hat{a}^\dagger \Delta\hat{a} \rangle} \right) + \xi(\tau). \quad (6)$$

The assumption of Gaussian statistics is not necessary, and as DENISOV, CASTRO-BELTRAN AND CARMICHAEL (2002) have shown, presumes detailed balance, which for some systems does not hold (see Sec. 2.3). It is only for this special case, though, that there is a direct and simple connection with the spectrum of squeezing.

The maximum signal to noise ratio is obtained with the coherent intensity much larger than the incoherent intensity,  $|\alpha|^2 \gg \langle \Delta\hat{a}^\dagger \Delta\hat{a} \rangle = \langle \Delta\hat{b}^\dagger \Delta\hat{b} \rangle$ . If, however, we choose the coherent offset in such a way that the coherent and incoherent intensities are the same,

$$|\alpha|^2 = \langle \Delta\hat{a}^\dagger \Delta\hat{a} \rangle = \langle \Delta\hat{b}^\dagger \Delta\hat{b} \rangle, \quad (7)$$

although one gives up a little in signal-to-noise ratio (a factor of  $\sqrt{2}$ ), one gains a different perspective in the discussion of nonclassical features in the correlation function. With the choice of maximal signal-to-noise ratio, and the mean field adjusted to be in phase with the local oscillator ( $\phi = \theta$ ), we obtain a normalized correlation function after dividing Eq. (6) by  $\sqrt{\eta 2\kappa} 2|\alpha|$  CARMICHAEL, CASTRO-BELTRAN, FOSTER AND OROZCO (2000),

$$h_\theta(\tau) = 1 + \frac{2}{1 + |\alpha|^2 / \langle \Delta \hat{a}^\dagger \Delta \hat{a} \rangle} \frac{\langle : \Delta \hat{a}_\theta(0) \Delta \hat{a}_\theta(\tau) : \rangle}{\langle \Delta \hat{a}^\dagger \Delta \hat{a} \rangle} + \frac{\xi(\tau)}{\sqrt{\eta 2\kappa} 2|\alpha|}. \quad (8)$$

In the limit of negligible residual shot noise ( $N_s \rightarrow \infty$ ), we denote the correlation function by

$$\bar{h}_\theta(\tau) = 1 + \frac{2}{1 + |\alpha|^2 / \langle \Delta \hat{a}^\dagger \Delta \hat{a} \rangle} \frac{\langle : \Delta \hat{a}_\theta(0) \Delta \hat{a}_\theta(\tau) : \rangle}{\langle \Delta \hat{a}^\dagger \Delta \hat{a} \rangle}. \quad (9)$$

The spectrum of squeezing (COLLETT AND GARDINER (1984), CARMICHAEL (1987)) may then be written as

$$S(\Omega, \theta) = 4F \int_0^\infty d\tau \cos(2\pi\Omega\tau) [\bar{h}_\theta(\tau) - 1], \quad (10)$$

where  $F = 2\kappa \langle \hat{a}^\dagger \hat{a} \rangle = 2\kappa(|\alpha|^2 + \langle \Delta \hat{a}^\dagger \Delta \hat{a} \rangle)$  is the input field photon flux. Thus,  $\bar{h}_\theta(\tau)$  achieves a time-resolved measurement of the quadrature amplitude fluctuations of the squeezed electromagnetic field. Notice that the measurement is independent of detection and collection efficiencies, though the efficiency  $\eta$  does appear in Eq. (8) as one of the factors affecting the single-to-noise ratio. The measured degree of squeezing also depends on the determination of the photon flux  $F$ . The technique is nevertheless less sensitive to efficiencies than traditional squeezing measurements (BACHOR (1998)) since the propagation losses are taken into account by the normalization of  $\bar{h}_\theta(\tau)$ .

Under the assumed conditions of Gaussian statistics,  $\bar{h}_\theta(\tau)$  is necessarily symmetric in time. We may then write the Fourier pair:

$$\begin{aligned} S(\Omega, \theta) &= 2F \int_{-\infty}^\infty d\tau \exp(i2\pi\Omega\tau) [\bar{h}_\theta(\tau) - 1], \\ \bar{h}_\theta(\tau) - 1 &= \frac{1}{4\pi F} \int_{-\infty}^\infty d\Omega \exp(-i2\pi\Omega\tau) S(\Omega, \theta). \end{aligned} \quad (11)$$

Notice that the photon flux plays a role, in inverse relationship, in the relative sizes of the spectrum of squeezing and the intensity-field correlation function. From this, it would seem that for large photon flux, nonclassical effects might be observed more readily in measurements of the spectrum

of squeezing, and for low photon flux, in measurements of  $h_\theta(\tau)$ . There is also a relationship between the time averaged  $\bar{h}_\theta(\tau)$  and the degree of squeezing at zero frequency, and between the frequency averaged spectrum of squeezing and  $\bar{h}_\theta(0)$ :

$$\begin{aligned} S(0, \theta) &= 2F \int_{-\infty}^{\infty} d\tau [\bar{h}_\theta(\tau) - 1], \\ \bar{h}_\theta(0) - 1 &= \frac{1}{4\pi F} \int_{-\infty}^{\infty} d\Omega S(\Omega, \theta). \end{aligned} \quad (12)$$

## 2.2. CLASSICAL BOUNDS FOR $H_\theta(\tau)$

Squeezing is directly related to a reduction in the variance of fluctuations in one of the field quadrature amplitudes. The squeezing manifests itself in the time domain through violations of classical bounds on the correlation function  $\bar{h}_\theta(\tau)$ . CARMICHAEL, CASTRO-BELTRAN, FOSTER AND OROZCO (2000) derived two such classical bounds whose derivation we review here.

We begin from the observation that the fluctuation intensity may be written as a sum of the normal-ordered variances for the quadrature field amplitudes:

$$\langle \Delta \hat{a}^\dagger \Delta \hat{a} \rangle = \langle : \Delta \hat{a}_\theta^2 : \rangle + \langle : \Delta \hat{a}_{\theta+\pi/2}^2 : \rangle. \quad (13)$$

Combining Eq. (9) with this result leads to an expression for  $\bar{h}_\theta(0)$  in the form

$$\bar{h}_\theta(0) - 1 = \frac{2}{1 + |\alpha|^2 / \langle \Delta \hat{a}^\dagger \Delta \hat{a} \rangle} \frac{\langle : \Delta \hat{a}_\theta^2 : \rangle}{\langle : \Delta \hat{a}_\theta^2 : \rangle + \langle : \Delta \hat{a}_{\theta+\pi/2}^2 : \rangle}. \quad (14)$$

In the classical case, both quadrature variances are greater than zero, so we may deduce both lower and upper bounds for  $h_\theta(0)$ :

$$0 \leq \bar{h}_\theta(0) - 1 \leq \frac{2}{1 + |\alpha|^2 / \langle \Delta \hat{a}^\dagger \Delta \hat{a} \rangle}. \quad (15)$$

The upper bound, in particular, is quite different from the familiar bounds on the intensity-intensity correlation function. Generalizing to non-zero time delay, we have the Schwarz inequality

$$|\langle : \Delta \hat{a}_\theta(0) \Delta \hat{a}_\theta(\tau) : \rangle|^2 \leq \langle : \Delta \hat{a}_\theta^2(0) : \rangle \langle : \Delta \hat{a}_\theta^2(\tau) : \rangle = \langle : \Delta \hat{a}_\theta^2 : \rangle^2, \quad (16)$$

which implies

$$|\bar{h}_\theta(\tau) - 1| \leq \frac{2}{1 + |\alpha|^2 / \langle \Delta \hat{a}^\dagger \Delta \hat{a} \rangle} \frac{|\langle : \Delta \hat{a}_\theta^2 : \rangle|}{\langle \Delta \hat{a}^\dagger \Delta \hat{a} \rangle}, \quad (17)$$

or

$$|\bar{h}_\theta(\tau) - 1| \leq |\bar{h}_\theta(0) - 1|. \quad (18)$$

This second condition and the lower bound in Eq. (15) are similar to the classical bounds associated with the definition of photon antibunching (KIMBLE, DAGENAIS AND MANDEL (1977), WALLS (1979), LOUDON (1980), PAUL (1982)).

For a classical field such that the intensity is much larger than the variance, one can prove in addition an inequality relating the intensity-field correlation function  $\bar{h}_\theta(0)$  and the intensity-intensity correlation function  $g^{(2)}(0)$ ; one finds

$$|\bar{h}_\theta(0)| \leq \sqrt{g^{(2)}(0)}, \quad (19)$$

If there is an offset field  $\alpha$  such that the intensity is equal to the variance, then the inequality is:

$$|\bar{h}_\theta(0)| \leq \sqrt{2g^{(2)}(0)}. \quad (20)$$

### 2.3. TIME REVERSAL PROPERTIES OF $H_\theta(\tau)$

The time symmetry of the cross-correlation of fluctuations about thermal equilibrium,  $\langle B(t+\tau)A(t) \rangle = \langle B(t-\tau)A(t) \rangle$ , where  $A$  and  $B$  are thermodynamic quantities, has a central place in statistical physics; it provides the fundamental basis for the Onsager relations (ONSAGER (1931), CASIMIR (1945)). The symmetry follows from microscopic reversibility ( $A$  and  $B$  are assumed both symmetric or antisymmetric under time reversal), which requires that the equilibrium state be maintained through detailed balance (TOLMAN (1938)). In quantum optics, one is usually concerned with steady states away from equilibrium, where correlation functions of the light emitted by an open system are measured through photoelectric detection. The detected radiation field is outgoing and absorbed by the environment; its steady state is thus manifestly not symmetric under time reversal. In a situation like this, fluctuations about the steady state may exhibit a specific time order.

The majority of studies in quantum optics have focused, nonetheless, on time-symmetric correlations. There are two main reasons for this. First, nonclassical phenomena such as photon antibunching and squeezing deal with autocorrelations,  $\langle A(t+\tau)A(t) \rangle$ , which are symmetric by definition for a stationary process. Second, although detailed balance is not required by microreversibility away from equilibrium (KLEIN (1955), TOMITA AND TOMITA (1973), TOMITA AND TOMITA (1974)), it may follow, nevertheless, from symmetry and boundary conditions (GRAHAM (1971)). A laser, for example, maintains its steady state through detailed balance (GRAHAM

AND HAKEN (1971)) in spite of the fact that it operates far from thermal equilibrium.

The cross-correlation of field intensity and amplitude provides, in principle, for the observation of time asymmetric correlations. Concerning the requisite failure of detailed balance, TOMITA AND TOMITA (1973) and TOMITA AND TOMITA (1974) determined what is needed in the case of Gaussian fluctuations: there must exist “a coupling between more than one degrees of freedom, so that there can be a *direction*” in the nonequilibrium flux through the system. Such a coupling—between the atom(s) and the cavity field—is a central feature in cavity QED. In the case of Gaussian fluctuations, however,  $h_\theta(\tau)$  reduces to the autocorrelation of Eq. (8), which is necessarily time symmetric. It follows that conditional detection of the kind considered can reveal time asymmetry only in a regime where the fluctuations are non-Gaussian (cross-correlating a “start” detection in one channel with homodyne detection in another provides wider possibilities). In this case a time asymmetric  $h_\theta(\tau)$  not only indicates a breakdown of detailed balance, it also provides direct evidence of non-Gaussian fluctuations.

We might expect resonance fluorescence to provide the simplest example of a time asymmetric  $h_\theta(\tau)$ ; its fluctuations are non-Gaussian and a coupling between degrees of freedom enters through the optical Bloch equations. Quantum transitions, on the other hand, occur between two states only; this suggests that detailed balance has to hold, since it is the only sort of balance that can maintain a steady state (KLEIN (1955)). It is indeed readily shown that  $h_\theta(\tau)$  is symmetric in resonance fluorescence.

The two-state restriction is lifted, on the other hand, for multiphoton scattering in cavity QED. In this context, DENISOV, CASTRO-BELTRAN AND CARMICHAEL (2002) recently computed time-asymmetric intensity-field correlation functions which demonstrate the breakdown of detailed balance. Examples of their results are presented in Sec. 3.2.3.

#### 2.4. INTENSITY-FIELD CORRELATIONS IN CLASSICAL OPTICS

In Chapter 8 of their celebrated book, MANDEL AND WOLF (1995) treat correlation functions of arbitrary order in the field, both even and odd orders. They develop Schwarz inequalities for cross-correlations of arbitrary order and show that in the case of Gaussian noise, the odd-order correlation functions are zero, the result we drew on in passing from Eq. (4) to (6). Moreover, when the field is quasi-monochromatic and the statistical ensemble characterizing the fluctuations is stationary—though not necessarily Gaussian—the odd-order correlations are zero except at very high orders.

The same authors treat quantum mechanical correlation functions of arbitrary order in Chapter 12 of their book, where they note that the odd-order correlation functions arise naturally in connection with nonlinear media. In these media the quantum expectation value of the intensity depends on odd-order correlation functions (involving unequal numbers of creation and annihilation operators). They show again, however, that when the electromagnetic field is stationary and quasimonochromatic, the odd-order correlations must vanish unless the order is very large.

The approach presented in 1 for the intensity-field correlation strictly speaking uses four fields: two for the intensity detection and two for the homodyne detection, except that the contributions of the strong local oscillator are averaged away.

### 3. Examples

The intensity-field correlation function has been calculated for three important sources of nonclassical light. We review the results in this section. The first is the Optical Parametric Oscillator (OPO) well below threshold (CARMICHAEL, CASTRO-BELTRAN, FOSTER AND OROZCO (2000)), where results for  $h_\theta(\tau)$  clarify how such a source of highly bunched light can nevertheless show quadrature squeezing. For the second, a cavity QED source, the intensity-field correlation captures the oscillatory exchange of excitation between the cavity mode and atoms, the normal-mode or polariton oscillation; the oscillation is related to the spectrum of squeezing (CARMICHAEL, CASTRO-BELTRAN, FOSTER AND OROZCO (2000)) and a discussion of its degradation through spontaneous emission is given (REINER, SMITH, OROZCO, CARMICHAEL AND RICE (2001)). The third example is a two-level atom coupled to the intracavity field of an OPO, which shows a mixture of the behavior demonstrated in the first two examples (STRIMBU AND RICE (2003)).

Various methods are available for calculating the intensity-field correlation function. Most directly, the two-time average in Eq. (4) may be evaluated from a knowledge of the source master equation,

$$\frac{d\rho}{dt} = \mathcal{L}\rho, \quad (21)$$

using the quantum regression formula. Generally, a different formula applies for positive and negative  $\tau$  (CARMICHAEL (1999)), allowing for the time asymmetry of Sec. 2.3. We have

$$\frac{\langle : \hat{S}(t) \hat{D}(t+\tau) : \rangle}{\sqrt{\eta 2\kappa} \langle \hat{S} \rangle} = \langle \hat{a}^\dagger \hat{a} \rangle^{-1} \begin{cases} \text{tr}[\hat{a} e^{-i\theta} e^{\mathcal{L}|\tau|} (\hat{a} \rho_{ss} \hat{a}^\dagger)] + \text{c.c.} & \tau \geq 0 \\ \text{tr}[(\hat{a}^\dagger \hat{a}) e^{\mathcal{L}|\tau|} (\hat{a} e^{-i\theta} \rho_{ss})] + \text{c.c.} & \tau \leq 0 \end{cases}, \quad (22)$$

where  $\hat{a}$  is related through Eq. (1) to the source quasimode  $\hat{b}$ .

Alternatively, a simulation of the conditional averaging process that yields the correlation function may be given within the framework of quantum trajectory theory. As is well known, the theory of quantum trajectories is formulated around the experimental data, viewed as a stochastic measurement record (CARMICHAEL (1993a)). For the detection scheme of Fig. 1, the record comprises the continuous homodyne current,  $I(t)$ , and the set of start times  $\{t_j\}$ . The source quasimode is in a quantum state  $|\psi_{\text{REC}}(t)\rangle$ , conditioned on this record. Realizations of  $I(t), \{t_j\}$ , and  $|\psi_{\text{REC}}(t)\rangle$  obey a set of stochastic differential equations that may be simulated on a computer. By sampling an ongoing realization of  $I(t)$ , one calculates the conditionally averaged photocurrent as

$$H_\theta(\tau) = \frac{1}{N_s} \sum_{j=1}^{N_s} I(t_j + \tau). \quad (23)$$

To carry out this program, the explicit quantum stochastic process (unravelling of the density operator  $\rho$ ) must be formulated in line with the principles introduced in Secs. 8.4 and 9.4 of CARMICHAEL (1993a), generalized in this case to include the coherent offset of Fig. 1 and to combine the continuous evolution under homodyne detection with the quantum jump conditioning,  $|\bar{\psi}_{\text{REC}}(t_j)\rangle \rightarrow \hat{a}|\bar{\psi}_{\text{REC}}(t_j)\rangle$ , at the start times  $t_j$  (the state  $|\bar{\psi}_{\text{REC}}(t)\rangle$  is not normalized). Clearly, in time step  $dt$ , the probability of a start count is  $(1 - \eta)2\kappa\langle(\hat{a}^\dagger\hat{a})(t)\rangle_{\text{REC}}dt$ . Between starts,  $|\bar{\psi}_{\text{REC}}(t)\rangle$  evolves according to the stochastic Schrödinger equation

$$d|\bar{\psi}_{\text{REC}}(t)\rangle = [(\hat{H}_S/i\hbar - 2\kappa A e^{-i\phi}\hat{b})dt + \sqrt{\eta\kappa}\hat{a}e^{-i\theta}dQ_t]|\bar{\psi}_{\text{REC}}(t)\rangle, \quad (24)$$

where  $\hat{H}_S$  is the non-Hermitian source Hamiltonian. The source state is conditioned through this equation on the ongoing realization of charge,

$$dQ_t = \sqrt{\eta 2\kappa}\langle\hat{a}_\theta\rangle_{\text{REC}}dt + dW_t, \quad (25)$$

deposited in the homodyne detector output circuit; the Wiener increment  $dW_t$  incorporates the shot noise. The simple filtering equation 26 introduces a realistic detection bandwidth  $\Gamma$ :

$$dI = -\Gamma(I dt - dQ_t). \quad (26)$$

If spontaneous emission is present, it may be incorporated in the usual way through additional quantum jumps.

The limit of weak excitation is a special case, since in this limit the correlation function is time symmetric and may be calculated from the

quantum trajectory equations by a straightforward analytical method. We write

$$|\psi_{\text{REC}}(t)\rangle = \sum_{n+\{m\}=0}^2 C_{n,\{m\}}(t)|n, \{m\}\rangle \quad (27)$$

where  $n$  denotes the photon number of the source quasimode, and  $\{m\}$  is the set of all other relevant quantum numbers (referring to the internal states of atoms in a cavity QED system, for example). Note that under the assumption of weak excitation, we may truncate the expansion at the level of two quanta. This is the minimal nontrivial truncation; one quantum is required to provide the “start” count, and at least one other is needed if there is to be a nontrivial conditional signal at the BHD. Note now that for weak excitation, the “start” counts are extremely infrequent on the time scale taken by the source to relax to its steady state. The time interval between one “start” and the next is then almost certain to be long enough for the steady state,

$$|\psi_{\text{REC}}^{\text{ss}}\rangle = \sum_{n+\{m\}=0}^2 C_{n,\{m\}}^{\text{ss}}|n, \{m\}\rangle, \quad (28)$$

to be reached. The approach to the steady state may be calculated from

$$\frac{d|\bar{\psi}_{\text{REC}}\rangle}{dt} = \frac{1}{i\hbar}\hat{H}_S|\bar{\psi}_{\text{REC}}\rangle, \quad (29)$$

where the terms proportional to  $\hat{a}$  and  $\hat{b}$  in Eq. (24) are neglected as higher order contributions. The conditional state after each “start” is now obtained as

$$|\psi_{\text{REC}}(t_j^+)\rangle \equiv \sum_{n+\{m\}=0}^1 C_{n,\{m\}}(t_j^+)|n, \{m\}\rangle = \frac{\hat{a}|\psi_{\text{REC}}^{\text{ss}}\rangle}{\sqrt{\langle\psi_{\text{REC}}^{\text{ss}}|\hat{a}^\dagger\hat{a}|\psi_{\text{REC}}^{\text{ss}}\rangle}}, \quad (30)$$

and solving Eq. (29) with this state as the initial condition yields

$$|\psi_{\text{REC}}(t_j + \tau)\rangle = \sum_{n+\{m\}=0}^2 C_{n,\{m\}}(t_j + \tau)|n, \{m\}\rangle. \quad (31)$$

From Eqs. (1), (28), and (31), we obtain

$$\langle\hat{a}_\theta\rangle_{\text{ss}} = \text{Re} \left[ \left( C_{1,\{m=0\}}^{\text{ss}} + Ae^{i\vartheta} \right) e^{-i\theta} \right], \quad (32)$$

$$\langle\hat{a}_\theta(t_j + \tau)\rangle_{\text{REC}} = \text{Re} \left\{ \left[ C_{1,\{m=0\}}(t_j + \tau) + Ae^{i\vartheta} \right] e^{-i\theta} \right\}, \quad (33)$$

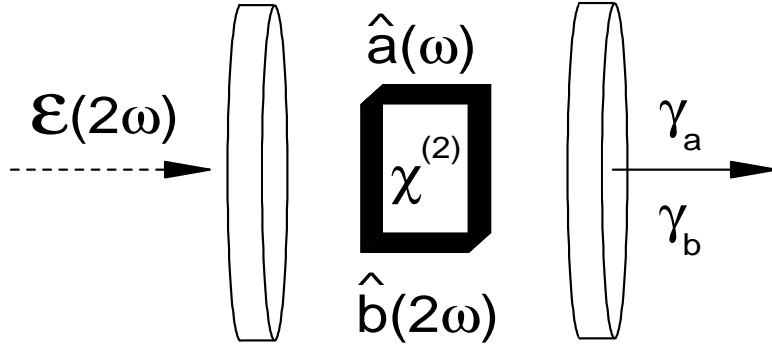


Figure 2. Schematic of the OPO. A classical drive  $\mathcal{E}$ , of frequency  $2\omega$ , injects energy into a cavity which contains a medium that has a nonlinear susceptibility  $\chi^{(2)}$ . The output is a field at the subharmonic frequency  $\omega$ .

and finally, taking the limit  $N_s \rightarrow \infty$  in Eq. (23) (also  $\Gamma \rightarrow \infty$ ), the result for the normalized correlation function is

$$\bar{h}_\theta(\tau) \equiv \frac{\bar{H}_\theta(\tau)}{\sqrt{\eta}2\kappa \langle \hat{a}_\theta \rangle_{\text{ss}}} = \frac{\text{Re} \left\{ \left[ C_{1,\{m=0\}}(t_j + \tau) + Ae^{i\vartheta} \right] e^{-i\theta} \right\}}{\text{Re} \left[ \left( C_{1,\{m=0\}}^{\text{ss}} + Ae^{i\vartheta} \right) e^{-i\theta} \right]}. \quad (34)$$

### 3.1. OPTICAL PARAMETRIC OSCILLATOR

Because of its simple nonlinearity, the process of parametric down conversion in a cavity has been the subject of extensive research in quantum optics. This process is the basis of the optical parametric oscillator (OPO), which is modelled (see Fig. 2) by two modes of the electromagnetic field, with frequencies  $\omega_a$  and  $\omega_b$ , and a nonlinear interaction proportional to  $i\hbar(\hat{a}^{\dagger 2}\hat{b} - \hat{a}^2\hat{b}^\dagger)$ . The Hamiltonian for the two coupled modes may be written as

$$H = \hbar\omega_a\hat{a}^\dagger\hat{a} + \hbar\omega_b\hat{b}^\dagger\hat{b} + \frac{i\hbar\chi}{2}(\hat{a}^{\dagger 2}\hat{b} - \hat{a}^2\hat{b}^\dagger). \quad (35)$$

Energy conservation requires that the frequencies are related, with  $\omega_b = 2\omega$ ,  $\omega_a = \omega$ . The coupling  $\chi$  between the modes is proportional to the second order nonlinear susceptibility of the medium,  $\chi^{(2)}$ . In addition to the interaction shown, the modes also couple to reservoirs with decay constants  $\gamma_a$  and  $\gamma_b$  to account for cavity loss, and there is a strong coherent drive  $\mathcal{E}$  of cavity mode  $\hat{b}$ . The OPO shows a point of instability as a function of the drive at  $\mathcal{E} = \mathcal{E}_{\text{th}} \equiv \gamma_a\gamma_b/\chi$ ; below this threshold the subharmonic mode has zero mean amplitude, while for  $\mathcal{E} > \mathcal{E}_{\text{th}}$  a nonzero mean field is established and parametric oscillation sets in.

The fluctuations in this system exhibit very large squeezing just below threshold (COLLETT AND GARDINER (1984), COLLETT AND GARDINER (1985)). Conditions of low photon flux, well below threshold where the squeezing is small, are of particular interest from the point of view of the intensity-field correlations. Although the squeezing is small, the output spectrum is a Lorentzian squared (COLLETT AND LOUDON (1987)), a manifestation of squeezing induced linewidth narrowing (RICE AND CARMICHAEL (1988)). The output intensity shows very large bunching as the photons are created in pairs, a condition that has been of interest for producing a conditional source of single photons for quantum cryptography.

With regard to the intensity-field correlation, conditions of low photon flux are of particular interest because they lead to extremely large violations of the upper bound of Eq. (15) (CARMICHAEL, CASTRO-BELTRAN, FOSTER AND OROZCO (2000)). The OPO with normalized pump parameter  $\bar{\mathcal{E}} \ll 1$ , ( $\bar{\mathcal{E}} \equiv \mathcal{E}/\mathcal{E}_{\text{th}}$ ) has quadrature variances and fluctuation intensity (MILBURN AND WALLS (1981))

$$\langle :(\Delta\hat{q}_X)^2: \rangle \approx \bar{\mathcal{E}}(1 + \bar{\mathcal{E}})/4, \quad (36)$$

$$\langle :(\Delta\hat{q}_Y)^2: \rangle \approx -\bar{\mathcal{E}}(1 - \bar{\mathcal{E}})/4, \quad (37)$$

and

$$\langle \Delta\hat{a}^\dagger \Delta\hat{a} \rangle = \langle :(\Delta\hat{q}_X)^2: \rangle + \langle :(\Delta\hat{q}_Y)^2: \rangle \approx \bar{\mathcal{E}}^2/2. \quad (38)$$

The ratio  $\langle :(\Delta\hat{q}_{X,Y})^2: \rangle / \langle \Delta\hat{a}^\dagger \Delta\hat{a} \rangle$  which enters on the right-hand side of Eq. (14) is of the order of  $1/\bar{\mathcal{E}}$ . If  $\bar{\mathcal{E}} \ll 1$ , the upper bound in Eq. (15) may be exceeded by orders of magnitude.

Figures 3i and ii illustrate this prediction for broadband detection. Well below threshold, where the squeezing is small (8% at line center), the classical bounds are violated dramatically. A violation exists for *both* quadratures of the field. It is permitted because of the anomalous phase of the fluctuation in Fig. 3ii, where, although the BHD current sampling is triggered by photon counts, the averaged data records a fluctuation that is *out of phase* with the offset; surely trigger counts would be more probable at the times of *in phase* fluctuations. The anomalous phase allows the sum of the quadrature variances to be much smaller than the modulus of either taken individually, and hence leads to the large violation of inequality (15).

The results displayed in Fig. 3 show that conditional homodyne detection is not simply an alternate method for the detection of squeezed light, but provides a completely different window on its nonclassicality. This is underlined by Fig. 4, where the violation of inequality (15) is *increasing* for decreasing pump parameter, while the squeezing and photon flux both decrease. For small  $\bar{\mathcal{E}}$ , CHD detects anomalously large fluctuations of the field amplitude which are *isolated in time* through the conditional measurement.

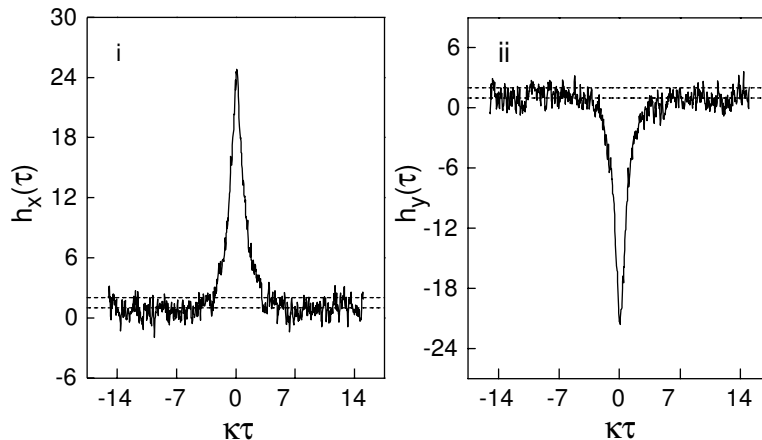


*Figure 3.* Quantum trajectory simulation of CHD for the OPO: (i)  $X$ -quadrature amplitude (unsqueezed), (ii)  $Y$ -quadrature amplitude (squeezed); with intracavity photon number  $\langle \hat{a}^\dagger \hat{a} \rangle = 2.0 \times 10^{-4}$  ( $\bar{\mathcal{E}} = 0.02$ ),  $\eta = 0.5$ ,  $N_s = 10,000$ . The dashed lines are the classical bounds.

It records only the real fluctuations associated with the rare two-photon pulses seen in direct photon detection. While the intensity-intensity correlation of the photon pulses is highly bunched and looks classical, with  $g^{(2)}(0) \sim 1/\bar{\mathcal{E}}^2$ , CHD resolves this correlation into quadrature amplitude components and uncovers the anomalous phase behavior at the level of the field amplitude.

In related work, several authors have used the beating of a local oscillator with a signal field on a beam splitter to enhance the ability to measure nonclassical effects such as photon antibunching and squeezing. This includes work by VOGEL (1991) on resonance fluorescence, and VYAS AND SINGH (2000) and DENG, ERENZO, VYAS AND SINGH (2001), and on the OPO. In the latter case, the output of the OPO mixed with the LO yields antibunched light, whereas it is highly bunched on its own. Neither of these schemes relies on a conditioned measurement. A scheme that does use a conditioned measurement to see antibunching in an OPO system has recently been proposed by LEACH, STRIMBU AND RICE (2003). SIDDIQUI, ERENZO, VYAS AND SINGH (2003) discuss conditional measurements as probes of quantum dynamics and show that they provide different ways to characterize quantum fluctuations in a subthreshold degenerate OPO.

### 3.2. CAVITY QED

We next consider a cavity QED system that consists of a single mode of the electromagnetic field interacting with a collection of two-level atoms

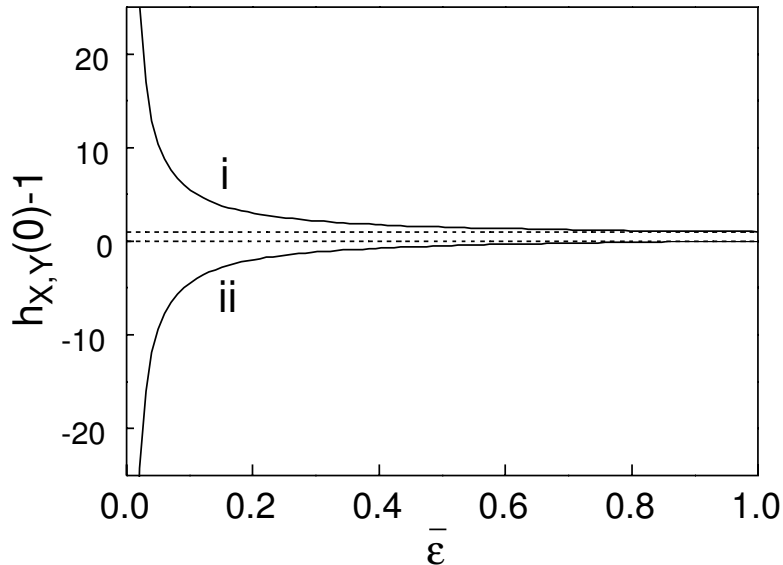


Figure 4. The intensity-field correlation at zero delay for the OPO:  $h_X(0) - 1$  (i) and  $h_Y(0) - 1$  (ii) as a function of normalized pump parameter  $\bar{\mathcal{E}}$ . The dashed lines are the classical bounds.

(see Fig. 5). Two spherical mirrors form an optical cavity that defines the field mode. A single or a few two level atoms are optimally coupled at rate  $g$  to the cavity mode. Dissipation occurs through decay of the field from the cavity at rate  $\kappa$  and decay of the atomic inversion  $\gamma_{\parallel} = 1/\tau$  ( $\tau$  is the radiative lifetime of the atomic transition) and polarization  $\gamma_{\perp}$ . For purely radiative decay,  $\gamma_{\parallel} = 2\gamma_{\perp}$ . The field  $\mathcal{E}/\kappa$  drives the system through one of the mirrors and it is possible to detect the light that escapes from the cavity mode through the output mirror.

The atom-cavity coupling rate is given by:

$$g = \left( \frac{\mu^2 \omega}{2\hbar \epsilon_0 V} \right)^{1/2} \quad (39)$$

for cavity mode volume  $V$ , atomic transition frequency  $\omega$ , and dipole moment  $\mu$ .

Work on Optical Bistability (OB) (LUGIATO (1984)) produced a large amount of experimental and theoretical literature on the transmission properties of an optical cavity filled with two-level atoms. Two dimensionless numbers from the OB literature are useful for characterizing cavity QED systems: the saturation photon number  $n_0$  and the single atom cooperativity  $C_1$ . Defined as  $n_0 = 2\gamma_{\perp}\gamma_{\parallel}/3g^2$  and  $C_1 = g^2/2\kappa\gamma_{\perp}$ , they scale the

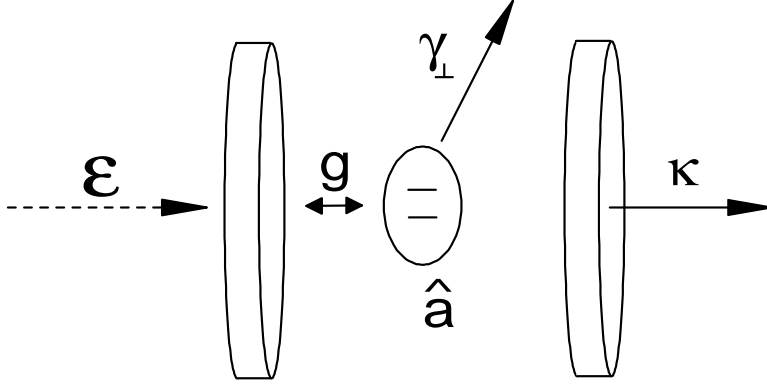


*Figure 5.* Schematic of Cavity QED a classical drive  $\mathcal{E}$  at frequency  $\omega$  injects energy into a single mode of the cavity cavity with one or more two-level atoms coupled to the cavity at a rate  $g$  with atomic decay  $\gamma$  and cavity decay  $\kappa$

influence of a photon and the influence of an atom in the system. The strong coupling regime of cavity QED  $n_0 < 1$  and  $C_1 > 1$  implies very large effects from the presence of a single photon and of a single atom in the system.

The Jaynes-Cummings Hamiltonian describes the interaction of a two-level atom with a single mode of the quantized electromagnetic field (JAYNES AND CUMMINGS (1963)),

$$\hat{H} = \hbar\omega_a\hat{\sigma}^z + \hbar\omega_c\hat{a}^\dagger\hat{a} - i\hbar g(\hat{\sigma}_+\hat{a} - \hat{a}^\dagger\hat{\sigma}_-), \quad (40)$$

where  $\hat{\sigma}_\pm$  and  $\hat{\sigma}^z$  are the Pauli spin operators for raising, lowering, and inversion of the atom, and  $\hat{a}^\dagger, \hat{a}$  are the raising and lowering operators for the field. The eigenstates for Eq. (40) reveal the entanglement between the atom and the field. The spectrum has a first excited state doublet with states shifted by  $\pm g$  from the uncoupled resonance.

The equilibrium state of the atom-cavity system is significantly altered by the escape of a photon. The dynamics consists of a collapse of the system state  $|\psi\rangle$  followed by a damped Rabi oscillation back to equilibrium. We are interested in the reduction of the equilibrium state of the cavity QED system after detecting a photon emitted from the cavity mode. Defining  $\hat{A}_\theta \equiv (\hat{a}\exp(-i\theta) + \hat{a}^\dagger\exp(i\theta))/2$ , where  $\hat{a}$  is the annihilation operator for the cavity field and  $\theta$  is the homodyne detector phase, we consider the quadrature amplitude,  $\hat{A}_{0^\circ}$ , in phase with the steady state of the field at low driving  $\lambda \equiv \langle \hat{a} \rangle = \mathcal{E}/[\kappa(1 + 2C)]$ . We limit the discussion to the case where the cavity and laser are resonant with the atomic transition. For weak excitation, and assuming fixed atomic positions the equilibrium state to second order in  $\lambda$  is the pure state (CARMICHAEL, BRECHA AND RICE (1991), BRECHA, RICE AND XIAO (1999))

$$\begin{aligned}
|\psi_{\text{ss}}\rangle = & [|0\rangle + \lambda|1\rangle + (\lambda^2/\sqrt{2})\chi\beta|2\rangle + \dots]|G\rangle \\
& + [\zeta|0\rangle + \lambda\zeta\beta|1\rangle + \dots]|E\rangle + \dots
\end{aligned} \tag{41}$$

where  $|G\rangle$  is the  $N$  atom ground state and  $|E\rangle$  is the symmetrized state for one atom in the excited state with all others in the ground state. We assume that all  $N$  atoms are coupled to the cavity mode with the same strength,  $g$ , with  $\chi$ ,  $\beta$  and  $\zeta$  derived from the master equation in the steady state (CARMICHAEL, BRECHA AND RICE (1991)):

$$\chi = 1 - 2C'_1; \quad \beta = \frac{1 + 2C}{1 + 2C - 2C'_1}; \quad \zeta = -\frac{\sqrt{N}g_0\lambda}{\gamma_\perp} \tag{42}$$

where:

$$C \equiv NC_1; \quad C'_1 \equiv \frac{C_1}{(1 + \gamma_\perp/\kappa)}. \tag{43}$$

After detecting the escaping photon, the conditional state is initially the reduced state  $\hat{a}|\psi\rangle/\lambda$ , which then relaxes back to equilibrium. The reduction and regression is traced by (CARMICHAEL, BRECHA AND RICE (1991), BRECHA, RICE AND XIAO (1999))

$$|\psi\rangle \rightarrow \{|0\rangle + \lambda[1 + \mathcal{A}\mathcal{F}(\tau)]|1\rangle + \dots\}|G\rangle + \dots, \tag{44}$$

where

$$\mathcal{A} = -\frac{4C'_1C}{1 + 2C - 2C'_1} \tag{45}$$

$$\mathcal{F}(\tau) = \exp\left(\frac{-(\kappa + \gamma_\perp)\tau}{2}\right) \left(\cos \Omega_0\tau + \frac{\kappa + \gamma_\perp}{2\Omega_0} \sin \Omega_0\tau\right) \tag{46}$$

$$\Omega_0 = \sqrt{g_0^2N - \frac{1}{4}(\kappa - \gamma_\perp)^2}. \tag{47}$$

From Eqs. 41 and 44 it is possible to see that after a photodetection, the quadrature amplitude expectation makes the transient excursion  $\langle \hat{A}_{0^\circ}(\tau) \rangle \rightarrow \lambda[1 + \mathcal{A}\mathcal{F}(\tau)]$  away from its equilibrium value  $\langle \hat{A}_{0^\circ} \rangle = \lambda$ .

In the weak driving limit, which assumes up to two excitations in the steady state of the system, the conditional field measurement is:

$$h_\theta(\tau) = (1 + \mathcal{A}\mathcal{F}(\tau)) \cos \theta. \tag{48}$$

The correlation function measures the coefficient of the single photon state in Eq. (44), it is usually a very small number and it is appropriate to talk of a field fluctuation at the sub-photon level.  $\mathcal{A}$  is the relative change of the field inside the cavity caused by the escape of a photon (CARMICHAEL,

BRECHA AND RICE (1991), REINER, SMITH, OROZCO, CARMICHAEL AND RICE (2001)): The limit of large  $N$  gives  $\mathcal{A} \approx -2C_1/(1 + \gamma_\perp/\kappa)$ , showing the importance of the single atom cooperativity as the parameter that establishes the non-classicality of the field. The sign of  $\mathcal{A}$  tells us that the cavity field goes negative causing a possible reduction.

Two dimensionless fields and intensities follow from the OB literature that allow to make contact with experiments: The intracavity field (intensity) with atoms in the cavity is given by  $x \equiv \langle \hat{a} \rangle / \sqrt{n_0}$ , ( $X \equiv \langle \hat{a}^\dagger \hat{a} \rangle / n_0$ ), and the field (intensity) without atoms in the cavity  $y \equiv \mathcal{E} / \kappa \sqrt{n_0}$ , ( $Y = y^2$ ), note that  $2\mathcal{E}^2/\kappa$  is the input photon flux.

### 3.2.1. *Low Field, weak driving limit*

Figure 6 presents results from REINER, SMITH, OROZCO, CARMICHAEL AND RICE (2001) with the intensity-field correlation function and the spectrum of squeezing for very low intensity; at most two excitations in the system. Both calculations are for a single atom maximally coupled using quantum trajectories. The size of the non-classicality of  $h(\tau)$  is very large and as it is the case with the OPO the size of squeezing is very small. There are very few fluctuations, but they are very large compared to the mean. A single photon fluctuation is too large compared to a saturation photon number of 0.01 and the system is driven with an intracavity intensity  $X \approx 3 \times 10^{-4}$ . The oscillations present are at the coupling constant  $g$ . The spectrum of squeezing is the so-called “vacuum Rabi” doublet (CARMICHAEL, BRECHA, RAIZEN, KIMBLE AND RICE (1989)); the fluctuations develop as spontaneous Rabi oscillations. The negative phase at  $\tau = 0$  of conditional field is responsible for the squeezing, otherwise there would be peaks instead of valleys at the Rabi frequency. The dashed line in Fig. 6ii is the spectrum of squeezing calculated directly from the quantum regression theorem. The solid line is the Fourier transform (see Eq. (10)) of Fig. 6i which comes from averaging the photocurrent from a quantum trajectory simulation over 55000 “starts”. Both approaches show the damped Rabi oscillations which precede and follow a photodetection. In the weak field excitation limit, RICE AND CARMICHAEL (1988) derived an analytical expression for the spectrum of squeezing (thin line in Fig. 6ii) which agrees with these results.

Figure 7i from REINER, SMITH, OROZCO, CARMICHAEL AND RICE (2001) shows the evolution of the field following the detection of a photon escaping through the cavity mode and Fig. 7ii shows the field evolution following the spontaneous emission of a photon out the side of the cavity. The collapse operation on the state  $|\psi\rangle$  of the type found in Eq. (44) is the dynamical mechanism which describes these two results.

These two distinct behaviors correspond fairly loosely to the regression

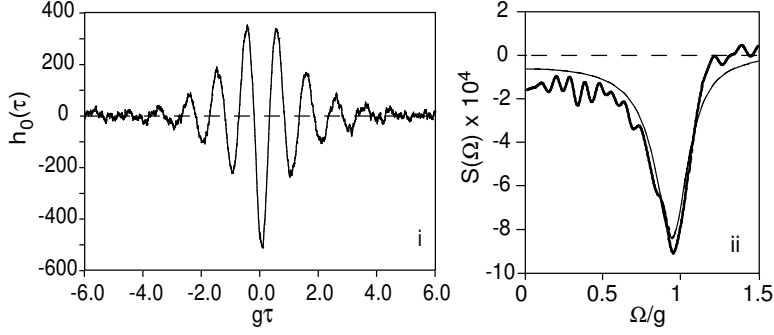


Figure 6. i. Intensity-field correlation  $h(0^\circ, \tau)$  from the quantum trajectory implementation of the conditioned homodyne detection for  $(g, \kappa, \gamma_\perp, \Gamma)/(2/\pi) = (38.0, 8.7, 3.0, 100)$  MHz,  $X = 2.99 \times 10^{-4}$ . ii. Spectrum of squeezing calculated from the cosine Fourier transform of  $h(0^\circ, \tau)$  in i. The continuous thin line is the exact spectrum of squeezing.

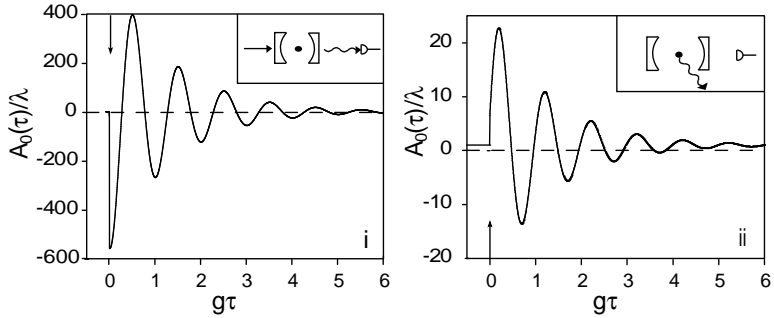
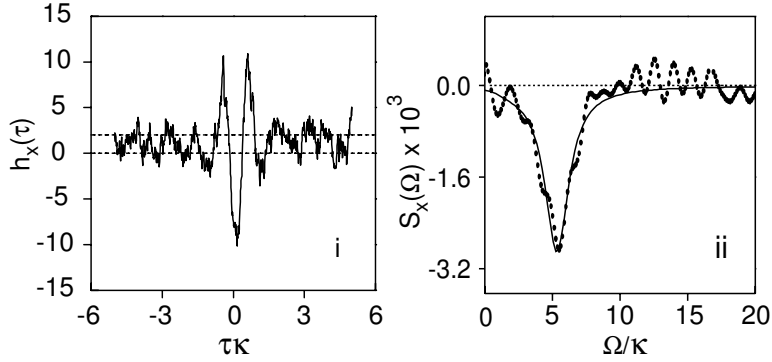


Figure 7. Regression of a cavity QED system back to steady state;  $N=1$ , low intensity i. after the detection of a photon escaping out of the cavity mode ii. after the escape of a photon through spontaneous emission. The inset shows the sequence of events in terms of the cavity QED system and the detector. The parameters used are the same as in Fig. 6.

to equilibrium observed in the step excitation in the field, Fig. 7i, and a step excitation in the atomic polarization, Fig. 7ii. Note the phase shift between the two responses. The steady state wavefunction determines the size of the steps. An undetected spontaneous emission produces the reduced state  $\hat{\sigma}^-|\psi\rangle/\lambda$ , which sets up a completely different evolution as shown in Fig. 7ii.

Quantum trajectories allow calculation with more than one atom and even permit to include the effects of an atomic beam. This approach gives a more accurate picture of the process in the laboratory. Fig. 8 from CARMICHAEL, CASTRO-BELTRAN, FOSTER AND OROZCO (2000) illustrates a calculation of the conditional field applied to cavity QED. Fig. 8i shows violations of the inequality from Eq. 15, while squeezing is evident from both the anomalous phase of the oscillation and the calculation of the spectrum of



*Figure 8.* Quantum trajectory simulation of CHD for many-atom cavity QED. i:  $X$ -quadrature amplitude (in phase with the mean field), the dashed lines are the classical bounds. Curve ii is the spectrum of squeezing obtained from the  $X$ -quadrature simulation.

squeezing from the Fourier transform of the  $x$  quadrature correlation function (Fig. 8ii). This calculation takes into account a typical transit time for an atomic beam experiment, dipole coupling constant  $g = 3.77\kappa$ , and atomic decay rate of  $\gamma = 1.25\kappa$ , intracavity photon number  $\langle \hat{a}^\dagger \hat{a} \rangle = 1.5 \times 10^{-4}$ ,  $\eta = 0.5$ ,  $N_s = 20,000$ , and an overall detection bandwidth of  $\Gamma = 10\kappa$ . The results for many atoms show that the predictions for one atom hold at a reduced size in an atomic beam.

### 3.2.2. High Field, outside the weak driving limit

The weak field calculations of the previous section make it clear that in the strong coupling regime a cavity emission will always produce a negative shift in the field. The ratio of the probability for a spontaneous emission to the probability for a cavity emission from steady state is

$$\frac{P_{\text{spont}}}{P_{\text{cavity}}} = 2NC_1. \quad (49)$$

Then in the strong coupling regime it is more likely for an atom to spontaneously emit out the sides of the cavity than for the cavity to emit a photon out through the exit mirror. Next we consider what happens in the likely event that a cavity photon follows a spontaneous emission.

Figure 9 from REINER, SMITH, OROZCO, CARMICHAEL AND RICE (2001) shows representative quantum trajectories calculated with two atoms in the cavity and the drive allows to have more than two excitations in the system, so we are outside the weak driving limit. In Fig. 9i the evolution starts with a spontaneous emission (A) out the side of the cavity, followed at (B) by a photon escaping through the cavity mode that gets registered

by the detector. The field jumps positive and changes curvature with the escaping cavity photon.

The driving field ( $\mathcal{E}/\kappa$ ), atom-field coupling ( $g$ ), and decay rates ( $\kappa, \gamma_{\perp}$ ) are such that the system is in a regime where the cavity field is bunched. Qualitatively, if there is a spontaneous emission event when the system has few excitations it returns to the steady state as in Fig. 6i. If the spontaneous emission event happens while in the bunched regime, followed by a cavity emission, then there are probably more excitations in the system. With one of the atoms removed from the system following the spontaneous emission, the probability for this energy to be in the cavity mode is increased. If there is a detection of a cavity photon soon after the spontaneous emission, then the system is in a regime where the intracavity field undergoes a large amplitude fluctuation, and the value of the cavity field is higher than the steady state value. This causes an upward jump in the expectation of the field. These types of events increase linearly with the number of atoms in the cavity, since the ratio of spontaneous emission events to cavity loss events is  $2NC_1$ .

The time evolution of the conditional field of the same system, driven much harder, shows multiple jumps; some from spontaneous emission and some from escapes through the mirror. The dynamics get very complicated and Fig. 9ii shows an example for illustration. The average value of the field from the conditional fluctuations still is much larger than the steady state in such cases.

Figure 9 demonstrates the insight that can be gained by studying individual trajectories. In this case, when the system is undergoing a large fluctuation, the intracavity photon number increases. This provides for a larger excited state population and higher probability of spontaneous emission, typically followed by a series of cavity emissions. Quantum trajectories give us insight into the underlying physics of the system which might not be evident from direct numerical solution of the master equation. Here we can see how spontaneous emission produces an incoherent field that can degrade the non-classicality of the correlation function and the squeezing.

The entire trajectory is a collection of events well separated in time of the type in Figs. 9i and 9ii. The average over many random realizations of these different events with an initial cavity emission setting the trigger at  $t = 0$ , recovers the conditioned field evolution.

Figure 10 shows results for two atoms maximally coupled to the cavity mode with a drive that corresponds to a steady state intracavity intensity of  $n/n_0 = 18$ , far from the low driving limit. The coupling constant  $g$  produces a similar vacuum Rabi oscillation  $\Omega_0$  as that of Fig. 6. The background that is visible in Fig. 10i around  $\tau = 0$  comes from the spontaneously emitted photons (REINER, SMITH, OROZCO, CARMICHAEL AND RICE (2001)). This

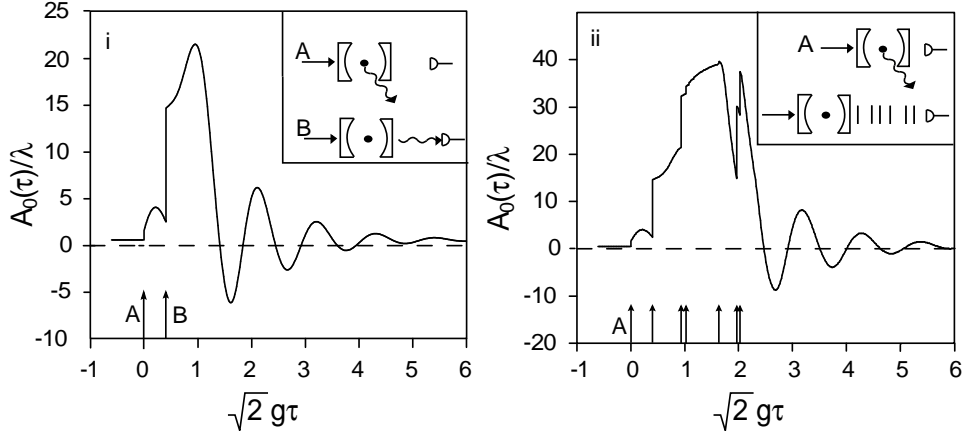


*Figure 9.* A quantum trajectory simulation which shows the time evolution of the field back to steady state after the detection of a photon. i. A spontaneous emission event followed by a cavity emission which starts the averaging process. ii. A spontaneous emission event followed by many cavity emission events. The inset shows the sequence of events in terms of the cavity QED system and the detector. Both figures were prepared with the following parameters:  $N = 2$ ,  $X = 18.1$ ,  $(g, \kappa, \gamma)/(2\pi) = (38.0/\sqrt{2}, 8.7, 3.0)$  MHz.

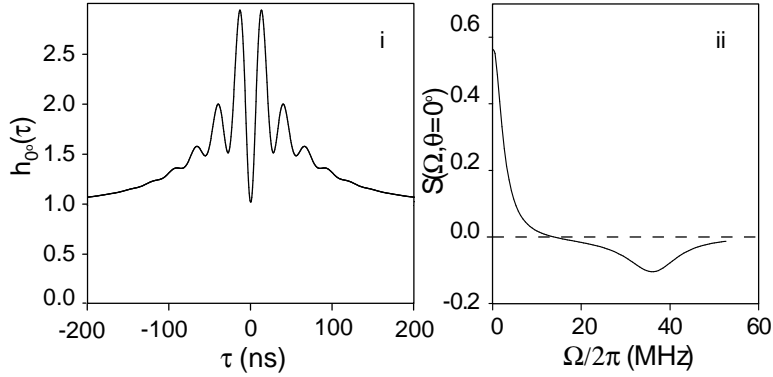


*Figure 10.* i:  $h_{0^{\circ}}(\tau)$  for  $N = 2$  atoms beyond the low intensity regime. ii: squeezing spectrum from the correlation function in i

background leads to a modification of the spectrum of squeezing, calculated from the symmetrized correlation function in Fig. 10i, shown in Fig. 10ii. Comparing the spectra in Fig. 6 to that of Fig. 10 a positive peak centered at the LO frequency ( $\Omega = 0$ ) has appeared, corresponding to the higher rate of spontaneous emission.

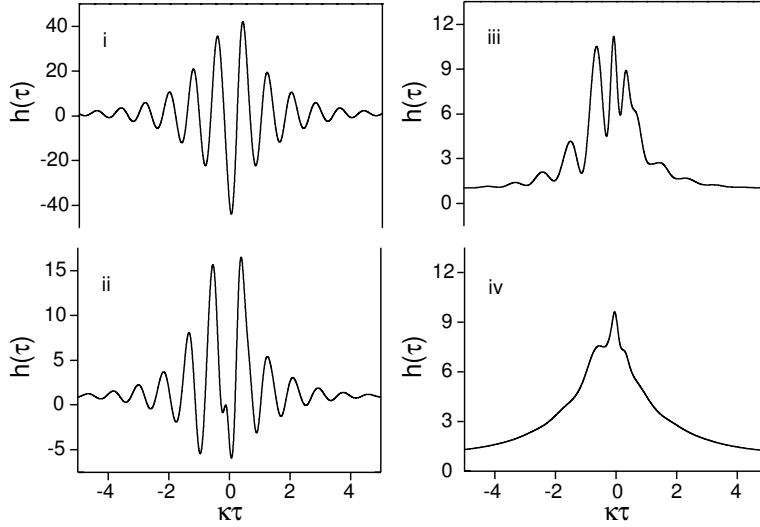


*Figure 11.* Time asymmetry in the cross-correlation of the intensity and field amplitude of the forwards scattered light in cavity QED. Results for one atom and no external noise. All curves are for  $\sqrt{Ng}/\kappa = 8$  and  $\gamma/\kappa = 1.25$  with intracavity photon numbers  $\langle \hat{a}^\dagger \hat{a} \rangle = 10^{-4}$  (i),  $10^{-3}$  (ii),  $10^{-2}$  (iii), and  $10^{-1}$  (iv).

### 3.2.3. Time asymmetry in cavity QED

Figures 11, 12, 13 present results of DENISOV, CASTRO-BELTRAN AND CARMICHAEL (2002) for the time asymmetry, that we mentioned before, of the correlation function for cavity QED. Here they have not made any assumptions about the nature of the noise. First they look at the pure system as they increase the drive strength of the external field in cavity QED in Fig. 11 [(i)-(iv)], and for increasing external noise in absorptive bistability in Fig. 12 [(i)-(iv)]. The two sets of results are selected for the qualitatively similar development. They do not correspond to the same operating parameters; although the decay rates and coupling strengths are matched. In both the weak and strong excitation limits the correlation functions are time symmetric. Time asymmetry is limited to a transition region of non-Gaussian fluctuations. Note how the oscillation is inverted and much bigger in Fig. 11 compared with Fig. 12. These distinctly nonclassical features are violations of the inequalities discussed earlier (See Eqs. 15 and 18).

Figure 13 shows results for many atom cavity QED without external noise. Again these results come from many realizations through quantum trajectories. The results are more similar to what happens in the laboratory FOSTER, OROZCO, CASTRO-BELTRAN AND CARMICHAEL (2000*a*), FOSTER, SMITH, REINER AND OROZCO (2002). Results are averaged over

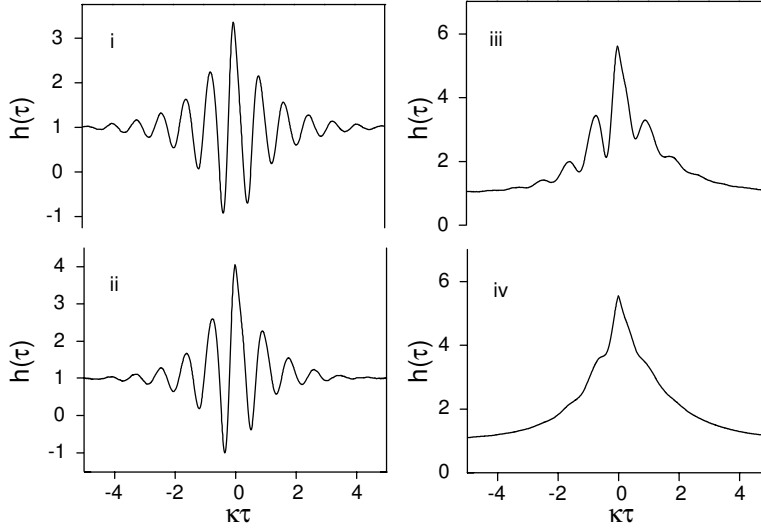


*Figure 12.* Time asymmetry in the cross-correlation of the intensity and field amplitude of the forwards scattered light in cavity QED. Results for  $N \gg 1$  atoms and amplitude noise on the external field. All curves are for  $\sqrt{N}g/\kappa = 8$  and  $\gamma/\kappa = 1.25$ ,  $Y = 13$  and noise strength  $2\Upsilon^2 = 25$  (i), 50 (ii), 80 (iii), and 120 (iv).

200 configurations of the five atoms most strongly coupled to a  $\text{TEM}_{00}$  standing-wave cavity mode [ $g_j = g \cos \theta_j \exp(-r_j^2/w_0^2)$ ] assuming a uniform spatial distribution of atoms: for  $\bar{N}_{\text{eff}} = 11$  atoms inside the mode waist,  $g_0/\kappa = 3.7$ ,  $\gamma/\kappa = 1.25$ , and mean intracavity photon numbers  $\langle \hat{a}^\dagger \hat{a} \rangle \approx 2.1 \times 10^{-3}$  (i) and  $7.3 \times 10^{-3}$  (ii). The main deficiency of the approximation is an overestimate of the dephasing caused by atomic beam fluctuations. In spite of this, time asymmetry is found in qualitative agreement with the experimental results (Figs. 3(a) and 4(b) of FOSTER, OROZCO, CASTRO-BELTRAN AND CARMICHAEL (2000a)); in particular, they reproduce the change in the sign of the asymmetry with increasing excitation strength.

### 3.3. TWO-LEVEL ATOM IN AN OPTICAL PARAMETRIC OSCILLATOR

STRIMBU AND RICE (2003) have considered the intensity-field correlation function for a two level atom in a degenerate optical parametric oscillator. They show large violations of the Schwartz inequalities in  $h(\tau)$ . We may view the system as an atom-cavity system driven by the occasional pair of correlated photons.

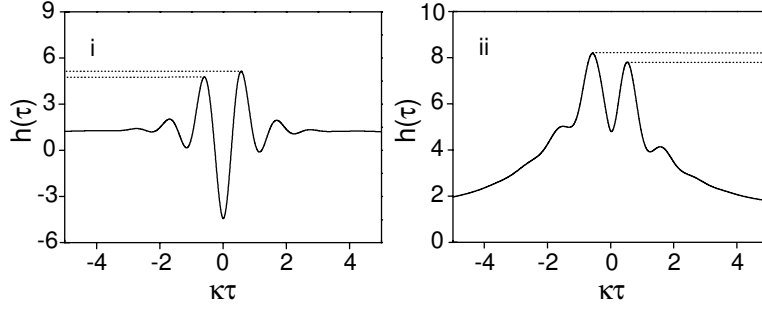


Figure 13. Time asymmetry in the intensity-field correlation in the output field for many-atom cavity QED without external noise. The dotted lines are for emphasis or the asymmetry.

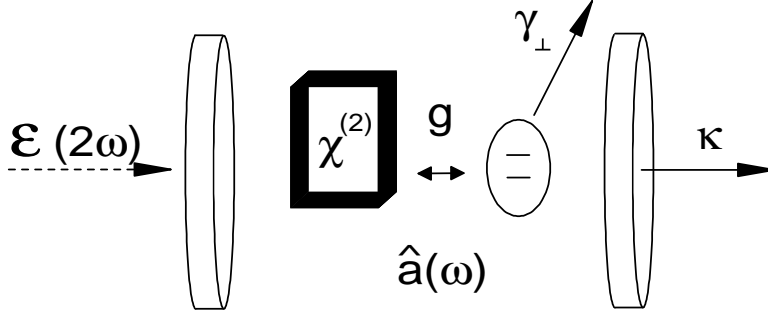


Figure 14. Two-level atom inside a driven optical parametric oscillator.  $\mathcal{E}$  is the driving field at frequency  $2\omega$ ,  $g$  is the atom-field coupling,  $\gamma$  is the spontaneous emission rate out the sides of the cavity, and  $2\kappa$  is the rate of intracavity intensity decay.

### 3.3.1. The physical system

Consider a single two-level atom inside an optical cavity, which also contains a material with a  $\chi^{(2)}$  nonlinearity. The atom and cavity are assumed to be resonant at  $\omega$  and the system is driven by light at  $2\omega$ . The system is shown in Fig. 14. The interaction of this driving field with the nonlinear material produces light at the sub-harmonic  $\omega$ . This light consists of correlated pairs of photons, or quadrature squeezed light. In the limit of weak driving fields, these correlated pairs are created in the cavity and eventually two photons leave the cavity through the end mirror or as out the side before the next pair is generated.

The system Hamiltonian is

$$H = i\hbar\mathcal{E}(\hat{a}^{\dagger 2} - \hat{a}^2) + i\hbar g(\hat{a}^{\dagger}\hat{\sigma}_- - \hat{a}\hat{\sigma}_+) + \hbar\omega(\hat{a}^{\dagger}\hat{a} + \frac{1}{2}\hat{\sigma}_z) \quad (50)$$

Here,  $g$  is the usual Jaynes-Cummings atom-field coupling defined in

Eq. 39 in the rotating wave and dipole approximations. The effective two-photon drive  $\mathcal{E}$  is proportional to the intensity  $I_{in}(2\omega)$  of a field at twice the resonant frequency of the atom (and resonant cavity) and the  $\chi^{(2)}$  of the nonlinear crystal in the cavity.

We use standard techniques to treat dissipation with a Liouvillian describing loss due to the leaky end mirror at a rate  $\kappa$  and spontaneous emission out the side of the cavity at a rate  $\gamma$ .

### 3.3.2. Discussion of the model

JIN AND XIAO (1993), JIN AND XIAO (1994) considered the spectrum of squeezing and incoherent spectra for this system. CLEMENS, RICE, RUNGTA AND BRECHA (2000) considered the incoherent spectrum in this system in the weak field limit, and found a variety of nonclassical effects. In the strong coupling regime, the incoherent spectrum consisted of a vacuum-Rabi doublet with holes in each sideband. Outside the strong coupling regime spectral holes and narrowing were reported. These were attributed to quantum interference between various emission pathways, which vanishes when the number of intracavity photons increases and the number of pathways increases.

As we are working in the weak driving field limit, we only consider states of the system with up to two quanta, i.e.  $|-, n\rangle$ ,  $|+, n\rangle$  where the first index denotes the number of energy quanta in the atoms ( $-$  for ground state, and  $+$  for excited state) and the second index corresponds to the excitation of the field ( $n$  = number of quanta). In this case we describe the system by a conditioned wave function, which evolves via a non-Hermitian Hamiltonian, and associated collapse processes. CARMICHAEL (1993a) These are given by

$$|\psi_c(t)\rangle = \sum_{n=0}^{\infty} C_{-,n}(t)e^{-iE_{-,n}t}|-, n\rangle + C_{+,n}(t)e^{-iE_{+,n}t}|+, n\rangle \quad (51)$$

$$H_D = -i\kappa\hat{a}^\dagger\hat{a} - i\gamma_\perp\hat{\sigma}_+\hat{\sigma}_- + i\hbar\mathcal{E}(\hat{a}^{\dagger 2} - \hat{a}^2) + i\hbar g(\hat{a}^\dagger\hat{\sigma}_- - \hat{a}\hat{\sigma}_+) \quad (52)$$

and collapse operators

$$C_{\text{cav.}} = \sqrt{\kappa}\hat{a} \quad (53)$$

$$C_{\text{spon.em.}} = \sqrt{\frac{\gamma}{2}}\hat{\sigma}_-. \quad (54)$$

For an initial trigger detection in the transmitted field, the appropriate collapsed state is given by

$$|\psi_c^T\rangle = \frac{\hat{a}|\psi_{SS}\rangle}{|\hat{a}|\psi_{SS}\rangle|} \quad (55)$$

In the weak field limit this becomes

$$|\psi_c^T\rangle = \frac{\sqrt{2}C_{-,2}^{SS} |-, 1\rangle + C_{+,1}^{SS} |+, 0\rangle}{\sqrt{2|C_{-,2}^{SS}|^2 + |C_{+,1}^{SS}|^2}} \quad (56)$$

Note there is no population in the ground state. Upon detection of a transmitted photon, as they are created in pairs, the system has one quanta, either in a cavity mode excitation (photon) or an internal excitation of the atom. In the weak field the probability of more than two quanta in the system initially is negligible; this is not the case for higher excitations. The certainty of the number of quanta is at the heart of all the nonclassical effects observed, these will vanish as the driving field increases. It is this driving of the system by the occasional pair of photons in an entangled state that creates most of the interesting effects. While this might be a difficult way to prepare such a state, by proper choice of  $g$ ,  $\kappa$ , and  $\gamma_\perp$ , any superposition of  $|+, 0\rangle$  and  $|-, 1\rangle$  may be created. After the detection, the system evolves in time,

$$|\psi_c^T\rangle = C_{-,1}^{CT}(\tau) |-, 1\rangle + C_{+,0}^{CT}(\tau) |+, 0\rangle \quad (57)$$

where the superscript  $CT$  indicates a collapse associated with a photon detection in transmission. The appropriate initial conditions are

$$C_{-,1}^{CT}(0) = \frac{\sqrt{2}C_{-,2}^{SS}}{\sqrt{2|C_{-,2}^{SS}|^2 + |C_{+,1}^{SS}|^2}} \quad (58)$$

$$C_{+,0}^{CT}(0) = \frac{C_{+,1}^{SS}}{\sqrt{2|C_{-,2}^{SS}|^2 + |C_{+,1}^{SS}|^2}} \quad (59)$$

In terms of the one-photon probability amplitudes,

$$h_\theta(\tau) = 1 + \frac{\sqrt{2}C_{-,1}^{CT}(\tau)C_{-,2}^{SS} + C_{+,0}^{CT}(\tau)C_{+,1}^{SS}}{\sqrt{2|C_{-,2}^{SS}|^2 + |C_{+,1}^{SS}|^2}} + \frac{C_{-,1}^{CT}(\tau) \cos \theta}{\sqrt{2|C_{-,2}^{SS}|^2 + |C_{+,1}^{SS}|^2}} \quad (60)$$

The first two terms are of order unity, while the third term is of order  $1/F$ . For weak fields, this term can be arbitrarily large, in violation of the inequality in Eq. (15)

### 3.3.3. Results

Figure 15i shows results from LEACH, STRIMBU AND RICE (2003) with a plot of  $h_\theta(\tau)$  for weak coupling ( $g/\gamma = 0.1$ ,  $g/\kappa = 0.02$ ), with cavity decay dominant over spontaneous emission ( $\kappa/\gamma = 5$ ); it presents large

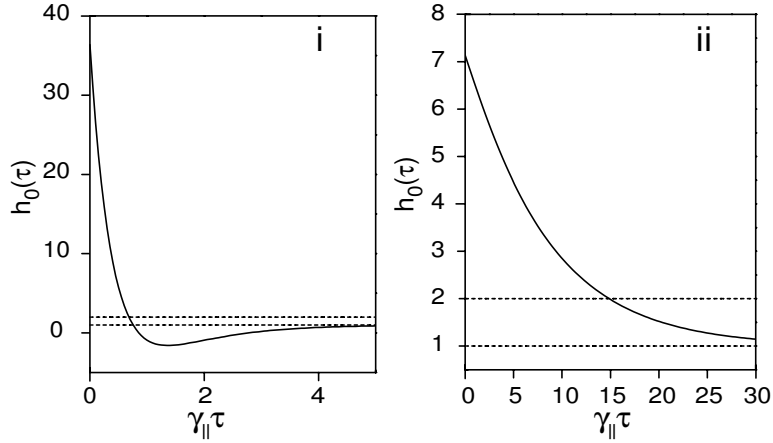


Figure 15. Plot of  $h_\theta(\tau)$  as a function of  $\gamma_{\parallel}\tau$  for weak coupling  $g$ . i  $\langle \hat{a}^\dagger \hat{a} \rangle = 3.8 \times 10^{-4}$ . ii  $\langle \hat{a}^\dagger \hat{a} \rangle = 2.0 \times 10^{-2}$ . The dashed lines indicate the range allowed for classical fields. See text for other parameters

violations of the inequality from Eq. (15), both above ( $h_\theta(\tau) > 2$ ) and below ( $h_\theta(\tau) < 0$ ). For the ordinary OPO, only the former is true. Fig. 15ii plots  $h_\theta(\tau)$  for weak coupling ( $g/\gamma = 0.1$ ,  $g/\kappa = 1.0$ ), with spontaneous emission dominant over cavity decay ( $\kappa/\gamma = 0.1$ ) and there are only violations above, as in the ordinary OPO. Fig. 16 shows results of the correlation function ( $h_\theta(\tau)$ ) in the regime of strong coupling: ( $g/\gamma = 5.0$ ;  $g/\kappa = 10.0$ ), there are large violations of the Schwartz inequality Eq. (15), both above and below, with the appearance of vacuum-Rabi oscillations.

The intensity-field correlation functions for transmitted fields of a two-level atom in an optical parametric oscillator in the weak field limit behaves essentially as a cavity QED system where an occasional pair of photons appears in the cavity and interacts with the system. For the intensity-field correlation function, which is essentially a quadrature field measurement conditioned on a photon detection, the system shows violations of the classical Schwartz inequality (Eq. (15)). Unlike the OPO without a two-level atom the system violates the upper and lower bounds over a wide range of parameters. Vacuum-Rabi oscillations appear for large Jaynes-Cummings couplings ( $g > \kappa, \gamma_{\perp}$ ). The inequality is violated from below only in the weak coupling regimes, and both above and below in the strong coupling regime. This is due in part to the field being  $\pi$  out of phase with the driving field. The nonclassical behavior tends to go away as the driving field is increased (i.e. more photons are present) or as atoms are added to the system.

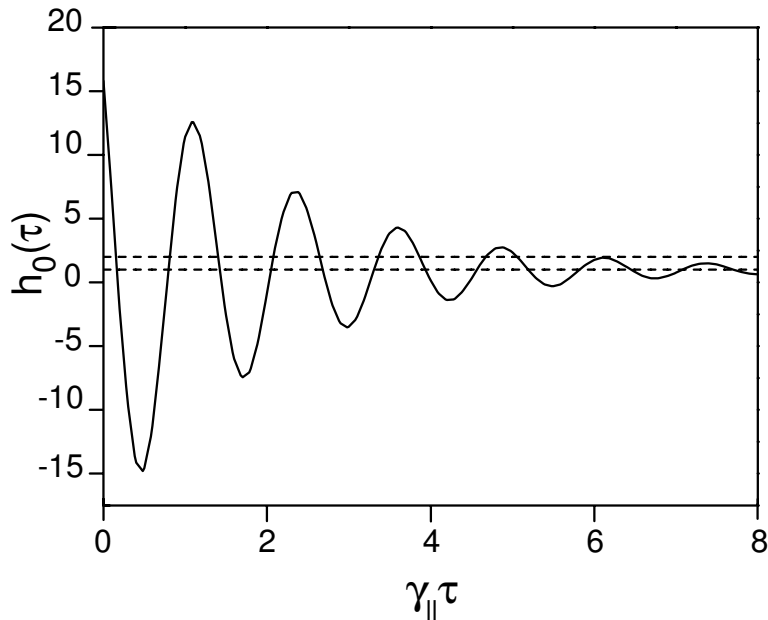


Figure 16. Plot of  $h_\theta(\tau)$  as a function of  $\gamma_{\parallel}\tau$  with strong coupling  $g$  and  $\langle \hat{a}^\dagger \hat{a} \rangle = 4.0 \times 10^{-4}$ . The dashed lines indicate the range allowed for classical fields. See text for other parameters.

#### 4. Experiment in Cavity QED

The experimental investigation of the intensity-field correlation function in cavity QED (FOSTER, OROZCO, CASTRO-BELTRAN AND CARMICHAEL (2000a), FOSTER, SMITH, REINER AND OROZCO (2002)) demonstrates the power of conditional homodyne detection. The measurement scheme detects the fluctuations of one quadrature of the cavity field as they happen in the laboratory. In this section we review the experimental results and present a description of the apparatus.

##### 4.1. CAVITY QED APPARATUS

The cavity QED system consists of a beam of optically pumped Rb atoms traversing a driven high finesse Fabry-Perot cavity. At its heart is the optical cavity. Piezo-electric transducers are attached to the cavity mirrors to provide control over the cavity length. During measurements, a feedback loop holds it on the TEM<sub>00</sub> resonance, where it supports a Gaussian standing wave mode with waist  $w_0 = 21 \mu\text{m}$  and length  $l = 410 \mu\text{m}$ . A one-sided configuration is used with 300 ppm transmission at the output mirror and 10 ppm transmission at the input mirror.

An effusive oven, 35 cm from the cavity, produces a thermal beam of Rb atoms in a chamber pumped by a large diffusion pump operated at typical pressures of  $1 \times 10^{-6}$  Torr. The oven is heated to  $\approx 430 \text{ K} \pm 0.1 \text{ K}$  with the help of computer controlled feedback. Final collimation is provided by a  $70 \mu\text{m}$  slit on the front of the cavity holder. The cavity is surrounded by a liquid nitrogen cooled Cu sleeve to reduce the background atomic vapor, as the presence of too much background destroys the observed correlations.

The excitation source is a Verdi 5 pumped titanium sapphire (Ti:Sapph) laser, a modified Coherent 899-01. The primary laser beam is split into a signal beam and auxiliary beams for laser frequency locking, cavity locking, and optical pumping. All beams are on resonance with the  $5S_{1/2}, F = 3 \rightarrow 5P_{3/2}, F = 4$  transition of  $^{85}\text{Rb}$  at 780 nm. The atoms are optically pumped into the  $5S_{1/2}, F = 3, m_F = 3$  state in a 2.5 Gauss uniform magnetic field applied along the axis of the cavity using the appropriate circular polarization of the pumping light.

The cavity is locked with a Pound-Drever-Hall scheme. During data collection, the laser beam traverses a chopper wheel which alternately passes the lock beam and opens the path from the cavity to the photon counting detectors at  $\approx 1.1 \text{ kHz}$ . Polarizing optics separate the signal from the lock. The signal beam is directed to the correlator. Between 50 and 85% of the signal emitted from the cavity is sent to the BHD. The remaining 50 to 15% of the signal goes to the avalanche photodiodes. The choice is guided by experimentally finding the best signal to noise ratio after averaging some 60,000 samples.

The three rates governing the atom-cavity coupling, cavity decay, and atomic decay in the cavity QED apparatus are  $(g, \kappa, \gamma_{\perp})/2\pi = (12, 8, 3) \text{ MHz}$ , which yield  $C_1 = 3$  and  $n_0 = 0.08$ , placing the experiment in the strong coupling regime of cavity QED. The measurements are carried out with an average intracavity field less than that of one photon.

## 4.2. CONDITIONAL HOMODYNE DETECTOR

Measurement of the intensity-field correlation requires a homodyne measurement of the signal to be made correlated with photon detections. A modified Mach-Zehnder interferometer was implemented to perform the measurement. Fig. 17 shows a schematic of the interferometer and its integration with the cavity QED apparatus. Light enters the Mach-Zehnder interferometer, driving the cavity QED system on one arm and providing a local oscillator (LO) for the BHD on the other (YUEN AND CHAN (1983a), YUEN AND CHAN (1983b)). A fraction of the signal is directed to the BHD and the remainder is sent to the intensity detector (avalanche photodiode APD). The photocurrent from the BHD is proportional to the

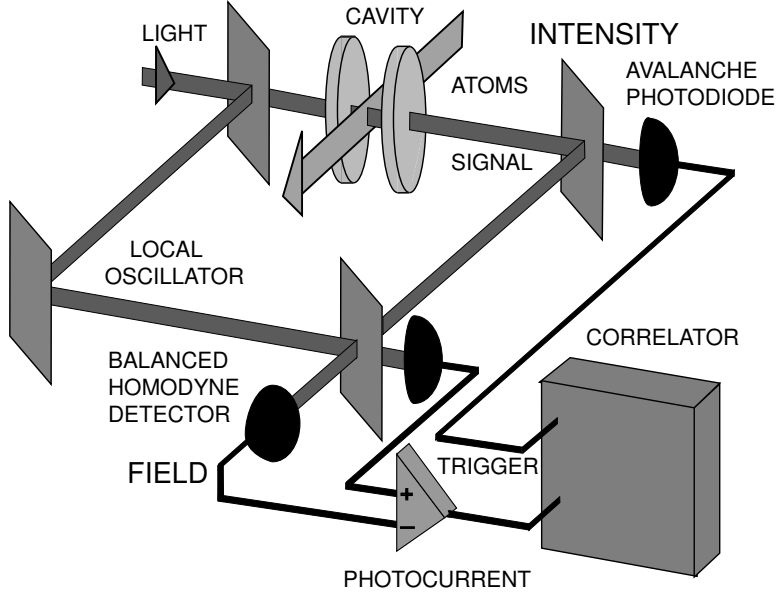


Figure 17. Schematic diagram of the cavity QED experimental setup.

LO-selected quadrature amplitude of the signal field. Photon detections at the APD are correlated with the BHD photocurrent to measure the intensity-field correlation function via Eq. (23). We discuss each component of the measurement in the following.

#### 4.2.1. Mach-Zehnder Interferometer

The Mach-Zehnder interferometer is used to separate the laser into a local oscillator and a signal beam which, although they follow separate paths, maintain a constant relative phase. Control of the relative phase is critical for the measurement. It is achieved by adjusting the path difference of the two arms with a piezo-actuated mirror and actively stabilizing the interferometer length with a feedback system. The stabilization uses a thermally stabilized He-Ne laser ( $\lambda = 633\text{nm}$ ) or diode laser ( $\lambda = 640\text{nm}$ ) locked using FM sidebands to an Iodine cell. The cavity QED system is transparent to the red wavelengths, but they form fringes at the Mach-Zehnder output. An edge filter separates the 780nm and red wavelengths at the output. The MZ length is continually adjusted so such that it sits at a red fringe maximum or minimum. A phase change may be introduced by locking the length to different red fringes. In this way the IR phase can be adjusted in steps of  $\delta\theta_{IR} = 146^\circ = (180^\circ \times 633/780)$ . There is also an optical path delay that can be mechanically adjusted to bring the IR and red in phase at

a particular fringe.

#### 4.2.2. *Amplitude Detectors*

The combined signal and LO field is directed to a pair of biased silicon photodiodes configured as a BHD. The AC coupled current from the photodiodes is amplified and subtracted to allow common mode rejection of local oscillator intensity noise (technical noise). The current from each detector first passes through a bias T which filters DC components below 100kHz. The DC component provides a direct measure of the local oscillator current.

#### 4.2.3. *Intensity Detectors*

The intensity detectors are arranged as a photon correlator consisting of two avalanche photodiodes (APD) behind an unpolarized 50/50 beam splitter. The detectors have a quantum efficiency of 50%, a dark count rate of less than 50Hz, and a 30ns dead time. The detector electronics produce a TTL pulse for each photon detection, a copy of which goes to a counter that measures the photon count rate of each APD. These rates yield the mean intensity of the light emitted from the cavity after correcting for efficiencies and linear losses.

#### 4.2.4. *Correlator Data Acquisition*

The homodyne current is sampled with a digital oscilloscope triggered by photon detections registered at the APDs. The trigger is produced by the apparatus used elsewhere for intensity correlation measurements (FOSTER, MIELKE AND OROZCO (2000*b*)). Instead of correlating the signals from the APDs, for the intensity-field correlation the two signals are combined in a logical OR. The digital oscilloscope samples the BHD photocurrent over a 500ns window at 2Gs/s with an 8 bit analog to digital (A/D) converter. It performs a summed average of the triggered samples. Typically up to  $5 \times 10^4$  samples are taken.

### 4.3. MEASUREMENTS

The saturation photon number  $n_0$  in the experiment is less than one and hence the observed fluctuations are associated with the emission of a single conditioning photon. Fig. 18 shows data taken at an intracavity intensity  $n/n_0 = 0.30$ , corresponding to a mean intracavity photon number of 0.027. The data is in the low intensity regime. The trace on the left is the unnormalized correlation function  $H(\tau)$ ; it shows non-classical behavior, violating the bound of Eq. (15), as the correlation has a minimum at  $\tau = 0$ . On the right is its FFT, which in accord with Eq. (10) is proportional to the spectrum of squeezing. The squeezing spectrum shows a dip at the

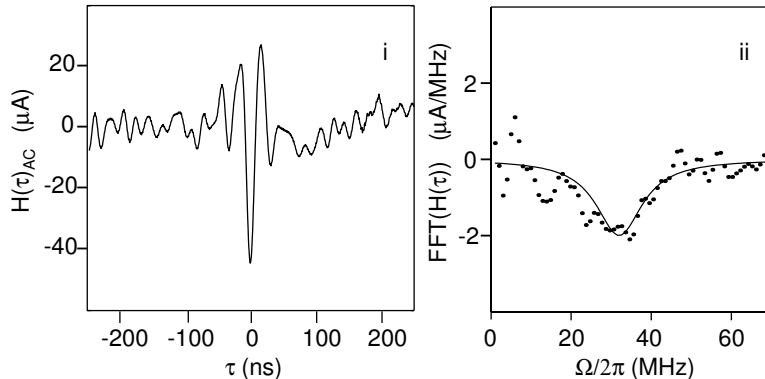


Figure 18. i Conditional field (unnormalized) at low Intensity ( $n/n_0 = 0.3$ ) Field Correlation and ii its Fast Fourier Transform.

vacuum Rabi frequency  $\Omega_0$ . There is qualitative agreement with the prediction of Fig. 6, although the data is not normalized as would be required for a quantitative comparison. The continuous line fitted to the FFT has the functional form predicted by the low intensity theory (REINER, SMITH, OROZCO, CARMICHAEL AND RICE (2001)).

The BHD measures the interference between the local oscillator and the emitted cavity field, which depends on their relative phase (Eq. (6)). A comparison of the conditionally averaged AC coupled photocurrent for two different local oscillator phases is shown in Fig. 19. When the relative phase is changed by  $146^\circ \approx 180^\circ$  (see Sect. 4.3.1) the sign of the interference changes. The normalization of these raw results is discussed in detail in the next section. Notice, however, that even without the normalization, the value of the field at  $\tau = 0$  in Fig. 19i is clearly smaller than its steady-state value. This is further evidence of a non-classical field, since it violates the lower bound of Eq. (15). This nonclassical feature demonstrates that the field fluctuations are anticorrelated in a similar way to the intensity in photon antibunching. Rather than seeing random field fluctuations, we see explicit evidence of the projection of the polarization field out of phase with the steady-state intracavity field.

#### 4.3.1. Normalization

The correlation function defined by Eq. (8) is normalized to the mean field; therefore, obtaining the proper normalization calls for precise knowledge of this field. As the detection system is AC coupled, the mean field must be determined in some indirect manner. In practice, the proper DC level and normalization has been determined by comparing the expected shot noise after averaging with the measured noise in the data. In this way, knowledge

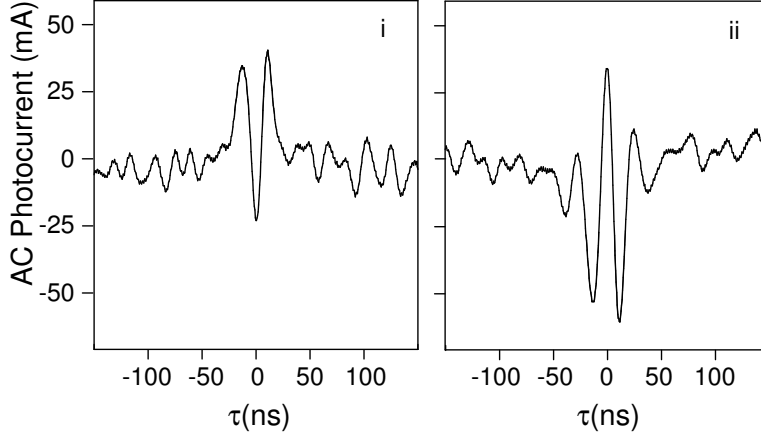


Figure 19. Plots i and ii are unnormalized homodyne averages with a phase difference of  $146^\circ$ .

of the averaging procedure allows the normalized correlation function to be extracted.

The noise amplitude for the normalized correlation function is given by

$$\delta h = \frac{1}{2\langle\hat{a}\rangle\sqrt{\eta}2\kappa}\sqrt{\frac{B\kappa}{2N_s}}, \quad (61)$$

where, as in Sec. 2,  $N_s$  is the number starts,  $\kappa$  is the cavity bandwidth,  $B$  is the detector bandwidth in units of the cavity bandwidth,  $\eta$  is the fraction of the output power sent to the BHD, and  $\langle\hat{a}\rangle$  is the mean intracavity field (no offset is used in this measurement). Assuming then that the data can be scaled with two constants,  $\Xi$  and  $\Upsilon$ , such that

$$h(\tau) = \Xi h_{\text{expt}}(\tau) + \Upsilon, \quad (62)$$

the normalization of  $h(\tau)$  requires that

$$\Xi h_{\text{expt}}(\infty) + \Upsilon = 1. \quad (63)$$

To determine  $\Xi$  we note that  $\Xi\delta h_{\text{expt}} = \delta h$ , and then assuming that the coherent transmission dominates the incoherent transmission ( $\langle\hat{a}\rangle \approx \sqrt{\langle\hat{a}^\dagger\hat{a}\rangle}$ ), Eq. (61) yields

$$\Xi \approx \frac{1}{4\delta h_{\text{expt}}}\sqrt{\frac{B}{\langle\hat{a}^\dagger\hat{a}\rangle\eta N_s}}. \quad (64)$$

$\Upsilon$  is then recovered from Eq. (63). Aside from the reasonable assumption, this method determines the scaling from quantities measured in the experiment. The number of starts is recorded on the digital oscilloscope. The intracavity intensity and  $\eta$  are obtained from the measured flux at the APDs,

and the detection bandwidth is determined by the 70 MHz low pass filter. The noise amplitude  $\delta h_{\text{expt}}$  is determined by taking the standard deviation of the unnormalized data.

A second approach to the normalization of  $h(\tau)$  uses the knowledge that the normalized field correlation is the square root of the intensity correlation  $g^{(2)}(\tau)$  in the weak field limit. This permits a DC level for the raw field measurement to be determined that properly scales the normalized intensity-field correlation function. The approach is less reliable for these particular measurements, however, because the data is not strictly taken in a weak field regime.

Finally, one might determine the normalization by calculating the DC field expected from the measured photon flux. From the measured flux, the expected DC voltage level can be calculated. Adding this level and dividing the total by the same mean level normalizes the correlation data to give a long-time mean of unity.

The difference between the first method of normalizing, on the basis of the expected noise, and the other two, is that it only includes the fraction of light directed to the BHD, without including the signal LO overlap, quantum efficiency, and additional losses. The first method of normalization was employed for the results presented here.

As an example of the normalized results, Fig. 20 shows  $h(\tau)$  for a larger intracavity intensity ( $n/n_0 = 1.2$ ). The dashed area in the figure marks the limits from the Schwartz inequalities in Eq. (15) and Eq. (18). The field is clearly non-classical. It is interesting to note that the intensity-intensity correlation function for an input intensity within 10% of that used to obtain Fig. 20 shows only classical fluctuations, in the form of significant photon bunching (FOSTER, OROZCO, CASTRO-BELTRAN AND CARMICHAEL (2000a)). Note that in comparison with Figs. 18 and 19 a significant background has appeared. Qualitatively the correlation function agrees with that in Fig. 10i, where the stronger driving field causes many spontaneous emissions which interrupt the oscillatory evolution of the system back to the steady state. REINER, SMITH, OROZCO, CARMICHAEL AND RICE (2001) study the effects of spontaneous emission in greater detail.

#### 4.3.2. *Spectrum of Squeezing*

The Fourier transform of the normalized intensity-field correlation function, when multiplied by the source photon flux, gives the spectrum of squeezing (Eq. (10)). Thus, a single time domain measurement of the fluctuation of the field quadrature amplitude yields the entire spectrum of squeezing in the frequency domain. The spectrum in Fig. 21 is computed from the normalized data of Fig. 20. Since the data contains noise, the time series was first symmetrized and then ordered in a one-dimensional array, with

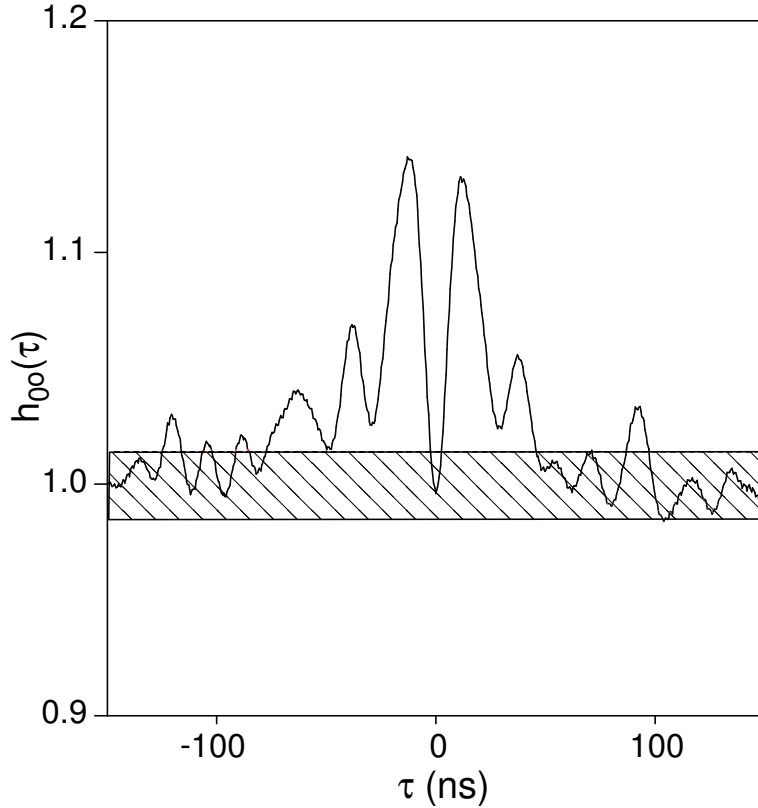


Figure 20. Measured normalized field correlation for an in-phase field in cavity QED.  $N=13$  and  $n/n_0 = 1.2$ . The dashed region is classically allowed.

the positive times appearing first followed by the negative times in reverse order. The real part of the fast Fourier transform (FFT) is then taken, and multiplied by the time resolution of the data and twice the flux  $F$  (Eq. (11)), as determined from the measured rates at the APDs and their measured efficiencies.

There is squeezing below the standard quantum limit (or the shot noise level) at the vacuum Rabi frequency  $\Omega_0$ . The magnitude at this frequency is  $\approx 5\%$ . The positive peak at zero is primarily caused by the spontaneous emission noise (REINER, SMITH, OROZCO, CARMICHAEL AND RICE (2001)) and is in qualitative agreement with the result displayed in Fig. 10.

The measurements of the cavity QED system show that the detection of a photon projects the system into a quantum state that evolves in time with a well-defined phase (relative to the mean field). The conditional homodyne detection uses this feature to observe the evolution of the field fluctuation; by triggering the collection of data from the BHD on a pho-

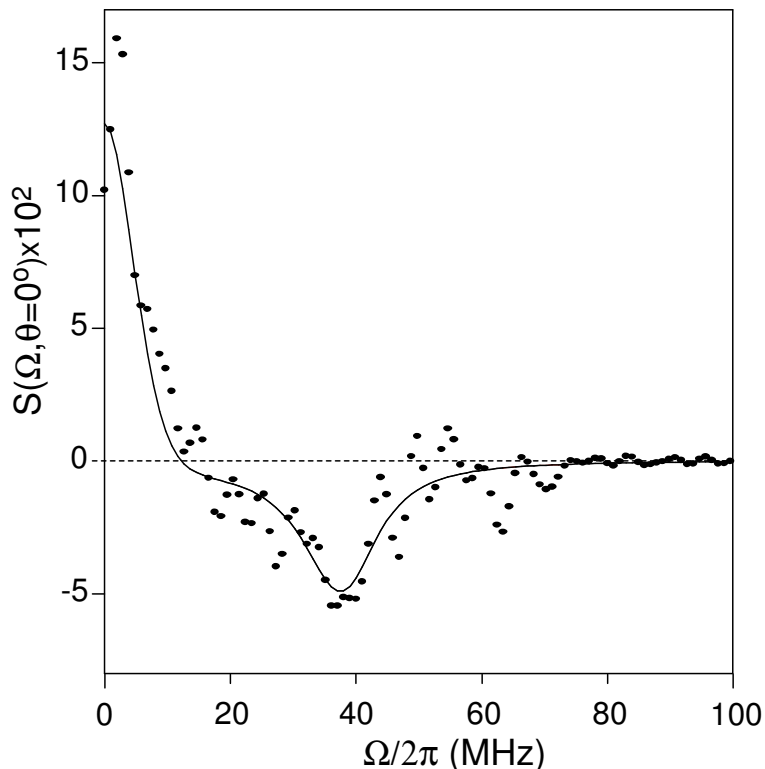


Figure 21. Squeezing Spectra for cavity system with  $n/n_0 = 1.2$ , and source flux  $F = 10.9 \times 10^6$  photons/sec.

ton detection, one recovers the subphoton field fluctuation from the large shot noise background. The time-domain measurement provides the information required to construct the full spectrum of squeezing in an efficiency independent manner.

## 5. Equal-Time Cross- and Auto-Correlations

We review in this section a series of theoretical and experimental papers that have studied conditional homodyne measurements at equal times, this means they do not look at the dynamics of the state as we have shown in previous sections, but they show very interesting results that demonstrate the quantum nature of conditional states of the electromagnetic field.

The entanglement available on the output field produced in the parametric down-conversion process has been exploited thoroughly to perform studies of conditional quantum measurements. YURKE AND STOLER (1987) proposed a cross correlation measurement, a conditional measurement, of the

quadrature of the electromagnetic field as a way to measure the amplitude probability distributions for photon-number operator eigenstates. BAN (1996) studied the photon statistics of conditional output states with a photon counting detector at one output of a beam splitter and a homodyne detector at the second output of the beam splitter for different input fields. This treatment is equivalent to  $h(0)$  the auto-correlation between the intensity and the field of a signal beam and enables the author to study the Mandel  $Q$  factor of the conditional output state in detail.

More recently CRISPINO, GIUSEPPE, MARTINI, MATALONI AND KANATOULIS (2000), and LVOVSKY, HANSEN, AICHELE, BENSON, MLYNEK AND SCHILLER (2001) performed a cross correlation measurement and applied tomographic methods to reconstructed the Wigner distribution for a one photon state using conditional homodyne detection. FIURASEK (2001) studied the photon statistics conditioned on the homodyne detection in a similar system. RESCH, LUNDEEN AND STEINBERG (2002a) and RESCH, LUNDEEN AND STEINBERG (2002b) used intensity-field cross-correlations for measurements of conditional coherence in prepared quantum states and to implement a conditional phase switch at the single photon level.

### 5.1. CROSS-CORRELATIONS

We generalize the definition of the unnormalized correlation function  $H_\theta(\tau)$  in Eq. 4 to allow two different modes, allowing us to cross correlate the intensity fluctuations on one mode with the field fluctuations of another mode:

$$H_\theta(\tau)_{i,j} = \frac{\langle : \hat{S}_i(t) \hat{D}_j(t + \tau) : \rangle}{\langle \hat{S}_i \rangle} + \xi(t). \quad (65)$$

where the labels  $i$  and  $j$  refer to two different modes. The normalization proceeds in the same way as in section 2 so we can now talk about the conditional field on mode  $j$  given a photon detection on mode  $i$ . This is useful in the case of the two entangled modes of a parametric down converter. (See Fig. 22). The connection with squeezing given by Eq. (10) for the auto-correlation  $h(\tau)$  is not valid in the case of the cross-correlation  $h(\tau)_{i,j}$ .

#### 5.1.1. Proposal for measuring the amplitude probability of a Fock state

YURKE AND STOLER (1987) present measurement strategy to obtain the probability distribution of an  $n$  photon Fock state. They suggest the highly correlated process of parametric down conversion where the number of photons counted by a photodetector in the idler beam during a coherence time could be used to gate a homodyne detector in the signal beam. The integrated output of the homodyne detector over a coherence time is only recorded when an  $m$ -photon wave packet enters its input port. In this way

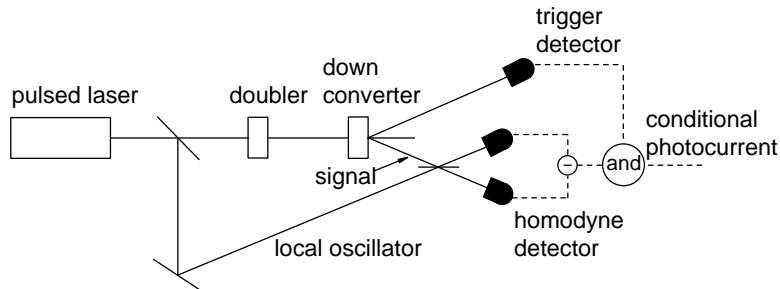


Figure 22. Simplified apparatus for measurement of the cross-correlation  $H(0)_{i,j}$  in parametric down conversion.

it is possible to map out the probability distribution for a field-amplitude component of a number-operator eigenstate.

They propose to measure the cross-correlation or conditional amplitude  $H(\tau)_{i,j}$  in a parametric down converter, where the idler beam is the mode  $i$ , and the signal beam is the mode  $j$ . Their proposal does not show a way to normalize the correlation function, as is suggested in Section 2 of this review by adding a coherent offset (See Fig. 1). They suggest that this conditional measurement could be used for the same purpose on other non-linear sources that produce non-classical light.

### 5.1.2. State Reconstruction of a Fock state and Quantum-Optical Catalysis.

CRISPINO, GIUSEPPE, MARTINI, MATALONI AND KANATOULIS (2000) and LVOVSKY, HANSEN, AICHELE, BENSON, MLYNEK AND SCHILLER (2001) have reconstructed the quantum state of optical pulses containing single photons using the method of phase-randomized pulsed optical homodyne tomography. The method they apply is very similar, but we review here in more detail the experiment of LVOVSKY, HANSEN, AICHELE, BENSON, MLYNEK AND SCHILLER (2001). They prepare a single-photon Fock state  $|1\rangle$ , in a well-defined spatiotemporal mode, using conditional measurements on photon pairs born in the process of parametric down-conversion following the original suggestion by YURKE AND STOLER (1987).

A single-photon counter is placed into one of the emission channels (labelled trigger in Fig. 22) to detect photon pair creation events and to trigger the readout of a homodyne detector placed in the other (signal) channel. (See HANSEN, AICHELE, HETTICH, LODAHL, LVOVSKY, MLYNEK AND SCHILLER (2001) for a description of their detector).

The signal beam as shown in Fig. 22 is not an optical beam in the traditional sense. The down-converted photons are in fact emitted randomly over a wide solid angle. The optical mode of the signal state is usable when

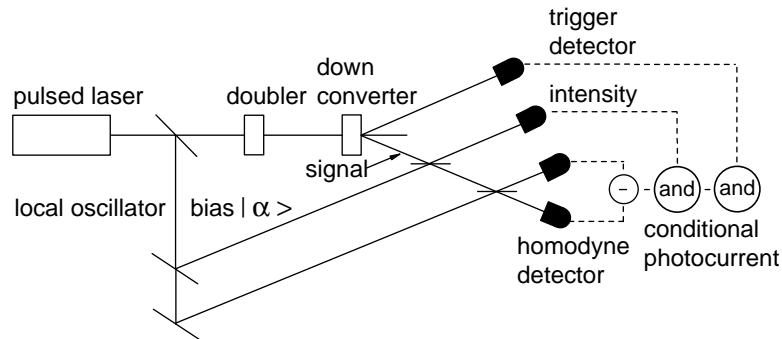


Figure 23. Simplified scheme of the experimental setup for  $H(0)$  of a Fock State with the help of an offset field.

a photon of a pair hits the trigger detector and is registered. Once the approximation of the Fock state is prepared, it is subjected to balanced homodyne detection YUEN AND CHAN (1983*a*), YUEN AND CHAN (1983*b*).

They obtain a probability distribution of the phase-averaged electric field amplitudes with a non-Gaussian shape. They then reconstruct the angle-averaged Wigner function from this distribution that shows a dip reaching classically impossible negative values around the origin of the phase space.

This is an intensity-field cross-correlation at equal times (see Eq. (65)), here presented as a conditional measurement. The evolution of the parametric down conversion process is very fast so they do not get the time dependence. They do not have an average field to normalize the correlation function that they measure, so the results are not independent of the quantum efficiency of the detectors.

LVOVSKY AND SHAPIRO (2002) have used the equal time intensity-field cross-correlations to measure and characterize non-classical light. Another use of the cross-correlation between the intensity of one mode and the field of another as done in the work described above is the work of FIURASEK (2001). Instead of conditioning on the intensity fluctuations (photodetection) the paper proposes to use the homodyne signal to condition the photodetections. The photodetector only counts if the absolute value of the measured idler quadrature lies inside a certain range. The conditioned generated signal is sub-Poissonian.

As a follow up of their previous cross-correlation work LVOVSKY AND MLYNEK (2002) use a intensity-field cross-correlator to measure the conditional field of a single photon. (See Fig. 23 for a schematic of their apparatus). They prepare the single photon through the parametric down conversion process with a conditional measurement and then they use the

Fock state as the “source” (See Fig. 1) for their intensity-field correlator. Since the Fock state does not have a steady state amplitude, they add a coherent bias field to do the auto-correlation measurement  $H_\theta(0)$  at equal times.

LVOVSKY AND MLYNEK (2002) show that with the appropriate choice of offset, they can prepare and characterize a coherent superposition states  $t|0\rangle + \alpha|1\rangle$  of the electromagnetic field by conditional measurements on a beam splitter. The single photon plays the role of a catalyst: it is explicitly present in both the input and the output channels of the interaction yet facilitates generation of a nonclassical state of light. Although their measurement does not give the full time dependent intensity-field correlation function, since they can obtain the value at  $\tau = 0$ , from the Fourier Transform relations presented in section 2 (see Eq. (12)) it is possible to obtain the integrated spectrum of squeezing for this Fock state.

## 6. Quantum Measurements and Quantum Feedback

The intensity-field correlation function has introduced a new way to analyze and study the non-classicality of the electromagnetic field. It does that mainly through the two Schwartz inequalities in Eqs. 15, 18. Recent works by WISEMAN (2002) and CARMICHAEL (2003) show that the conditional homodyne detection, key to measuring  $h(\tau)$ , has further implications in the quantum theory of measurement through its relationship with the weak measurements of Aharonov, and in distinguishing *qualitatively* between vacuum state squeezing and the mere squeezing of classical noise. CARMICHAEL (in press) has used the connection between the intensity-field correlation and the particle-wave aspects to further elucidate this important question. Conditional measurements and quantum feedback are intimately related WISEMAN (1994). The last part of this section presents a proposal to use CHD in quantum feedback to modify the the response of a cavity QED system.

### 6.1. WEAK MEASUREMENTS

We review the main ideas behind a weak measurement and follow WISEMAN (2002) in developing the connection between  $h(\tau)$  and weak measurements. A weak measurement is one that minimally disrupts the system, while consequently yielding a minimal amount of information about the observable measured (AHARONOV, ALBERT AND VAIDMAN (1988)). For a given initial system state, the ensemble average of weak-measurement results is the same as for strong i.e., projective measurement results. Where weak measurements are interesting is when a final as well as an initial state is specified. Here the final state is the result of a second measurement (a strong one), so

that the ensemble average is taken over a postselected ensemble, in which the desired result for the final measurement was obtained.

A homodyne measurement gives a current proportional to the expectation value of the quadrature operator and so conditions the system state. The photon counting also gives a continuous measurement that is weak in the sense that the average change in the conditioned system in time  $\delta t$  is of order  $\delta t$ , as seen in quantum trajectories (REINER, SMITH, OROZCO, CARMICHAEL AND RICE (2001)). However, unlike homodyne detection, sometimes the change is great, there is a quantum jump and either the system changes state or continues its evolution.

Looking at the negative time side of the correlation function it is possible to see that this is a weak value preselected by the system being in its stationary state, and postselected on the photon detected at time  $\tau = 0$ . The measurements of the correlation function, as a function of time shows the dynamics of a weak value (quadrature of the electromagnetic field) over time. The strangeness of the weak values in this experiment is not surprising, since the conditions set by AHARONOV, ALBERT AND VAIDMAN (1990) are fulfilled. That is, the postselection is done on a rare event, the detection of one photon rather than zero photons.

The formulation of the quantum trajectory has to have the influence of the homodyne detection to be consistent and describe the times before the detection of a photon. WISEMAN (2002) shows that  $h(\tau)$ , the intensity-field correlation function reduces to a form as simple as that originally derived by AHARONOV, ALBERT AND VAIDMAN (1988)

## 6.2. VACUUM STATE SQUEEZING VERSUS SQUEEZED CLASSICAL NOISE

It is apparent from Eqs. (9) and (10) that conditional homodyne detection offers a somewhat different view of squeezed light than the conventional squeezing measurement. Certainly, the latter is usually carried out in the frequency domain, but this difference is not important. In both cases we have a Fourier relationship between frequency and time of the sort given in Eq. (11). The important difference is that in the conventional measurement, the relevant temporal correlation function is the direct autocorrelation of the current,  $i(t)$ , from the balanced homodyne detector, which is calculated from a symmetrically ordered quantum average, rather than the normal-ordered average of Eq. (9). The difference is a direct manifestation of conditioning, and from it, it follows that whereas a conventional homodyne measurement distinguishes quantitatively between vacuum state squeezing and squeezed classical noise, conditional homodyne detection distinguishes quantum from classical squeezing in a qualitative way (CARMICHAEL (2003)).

Physically, in any realistic example, squeezing is restricted to a finite bandwidth, outside of which the field fluctuations are not squeezed. For vacuum state squeezing, the unsqueezed fluctuations appear as shot noise on  $i(t)$ , the shot noise commonly being interpreted as a manifestation of the vacuum fluctuations of the measured field. If, in addition, this field carries broadband classical noise, the unsqueezed classical fluctuations also add to the fluctuations of  $i(t)$ . Thus, in a conventional squeezing measurement, unsqueezed classical noise *and* shot noise contribute to the autocorrelation of  $i(t)$ . In conditional homodyne detection, by comparison, only the classical noise contributes; the shot noise is eliminated; through the conditional sample average, the term  $\xi(\tau)$  in Eq. (9) is reduced (in the ideal limit) to zero.

To illustrate the comparison, we consider the squeezing of broadband classical noise, as depicted in Fig. 24i. Classical noise of bandwidth (halfwidth)  $B_c\kappa = 15\kappa$  is squeezed by a sub-threshold degenerate parametric oscillator over the bandwidth  $\kappa$ . Fluctuations on the squeezed quadrature of  $E_{\text{out}}$  are then measured using either conventional homodyne detection or conditional detection; the detection bandwidth is  $B_d\kappa = 25\kappa$ . Figures 24ii and iii show simulated results for the direct autocorrelation of the homodyne current, and thus provide the time-domain view of a conventional squeezing measurement. The presence of squeezing is evident from the broad negative dip, while fluctuations outside the squeezing bandwidth produce the narrow spike around  $\tau = 0$ . In frame ii, this spike is contributed to by both classical fluctuations and shot noise. The shot noise alone contributes in frame iii; here the height of the spike is correspondingly reduced.

For comparison, Fig. 25 displays simulated results of conditional homodyne detection. In this case, there is no shot noise contribution to the central spike. The spike shrinks and eventually disappears as the classical noise level is decreased. A central spike in  $h_\theta(\tau)$  is therefore a qualitative indicator of the squeezing of classical, as opposed to vacuum state noise.

CARMICHAEL (2003) has also investigated to what extent stochastic electrodynamics is able to reproduce this distinction between classical and vacuum noise squeezing. He finds that the results of Fig. 25 are reproduced, but with an additional background contribution generated by “starts” induced by the explicit vacuum noise (unphysical dark counts). In related work, triple correlations of the quadratures of the electromagnetic field have been used by DRUMMOND AND KINSLER (1995), KINSLER (1996), CHATURVEDI AND DRUMMOND (1997), and POPE, DRUMMOND AND MUNRO (2000) to investigate differences between the predictions of stochastic electrodynamics and quantum mechanics. They compare the former with the positive  $P$  representation and also focus their attention on the parametric oscillator.

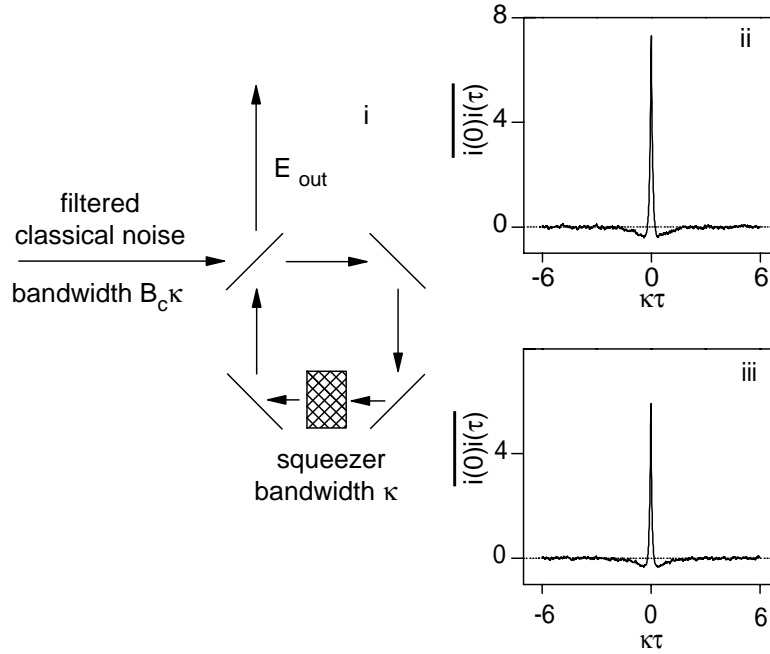


*Figure 24.* i Sketch of the degenerate OPO squeezer with broadband classical noise input. Under conventional homodyne detection of the field  $E_{out}$  [ii and iii], the autocorrelation of the homodyne current reveals nonsqueezed fluctuations over a wide bandwidth (central spike) and a narrow bandwidth of squeezed fluctuations (negative dip): for a classical noise bandwidth  $B_c \kappa = 15\kappa$ , detection bandwidth  $B_d \kappa = 25\kappa$ , and classical noise photon numbers (in the degenerate OPO cavity) of ii  $\bar{n}_c = 0.2$  and iii  $\bar{n}_c = 0$ ; the degenerate OPO squeezer is operated at 40% of threshold.

### 6.3. APPLICATION OF $H_\theta(\tau)$ TO QUANTUM FEEDBACK

Most quantum feedback proposals use the BHD photocurrent to modify the drive acting on a quantum system. The goal of such feedback can vary from reducing out-of-quadrature noise (TOMBESI AND VITALI (1995)) to modifying the system dynamics (WANG AND WISEMAN (2001)). All these proposals rely on continuous feedback. DOHERTY AND JACOBS (1999) showed that one can improve these schemes with knowledge of the conditioned state. A recent experiment by SMITH, REINER, OROZCO, KUHR AND WISEMAN (2003) shows the success of quantum feedback in a strongly coupled system through conditional intensity measurements.

We consider adding feedback to the single atom cavity QED system (See section 3.2 for theoretical details). A photon leaves the cavity which initiates a fluctuation. Conditioning the BHD detectors to observe this fluctuation also creates the opportunity to apply feedback.

The dynamics of this system, once the detection of the photon is made,

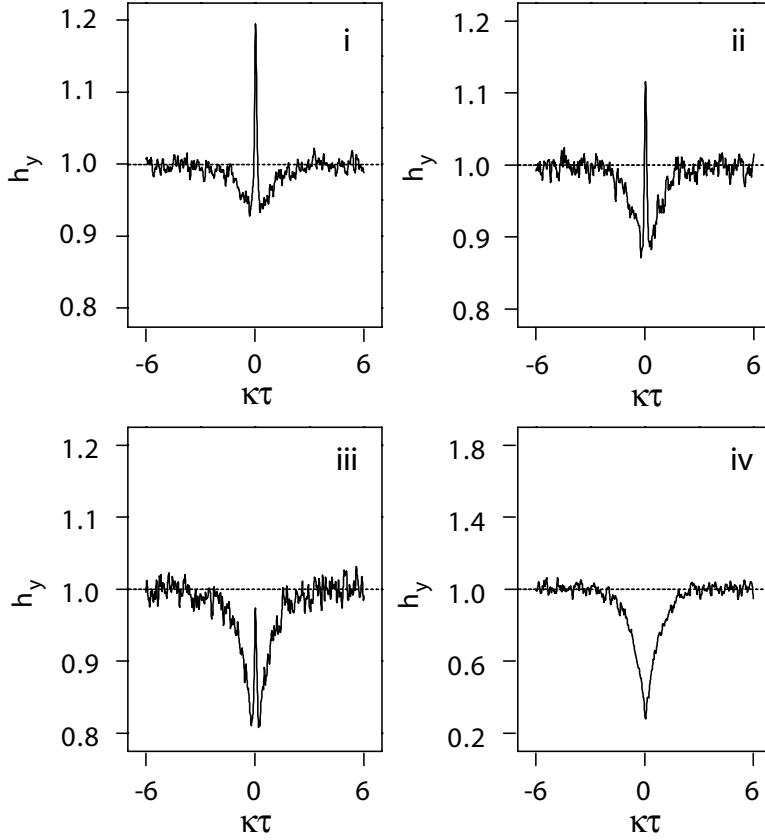


Figure 25. Broadband classical noise squeezing under conditional homodyne detection. The correlation function  $h_Y(\tau)$ , with  $Y$  the squeezed quadrature, is plotted for the parameters of Fig. 24 and classical noise photon numbers (in the degenerate OPO cavity) of i  $\bar{n}_c = 0.2$ , ii  $\bar{n}_c = 0.1$ , iii  $\bar{n}_c = 0.05$ , and iv  $\bar{n}_c = 0$ .

are governed by the regression to steady state of the field. That for weak fields reduce in the Optical Bistability notation of LUGIATO (1984) to:

$$\begin{aligned}\dot{x} &= \kappa y + gp - \kappa x + \mathcal{G}x \\ \dot{p} &= -gx - \gamma_{\perp} p.\end{aligned}\quad (66)$$

where  $y$  is the normalized intracavity field in the absence of atoms (proportional to the drive),  $x$  the intracavity field in the presence of atoms,  $p$  is the atomic polarization, and  $\mathcal{G}$  quantifies the strength of the field feedback.

The intensity-field correlator measures the conditioned BHD photocurrent,

$$i(t) = \sqrt{2\kappa\eta}\langle x(t) \rangle + \xi(t), \quad (67)$$

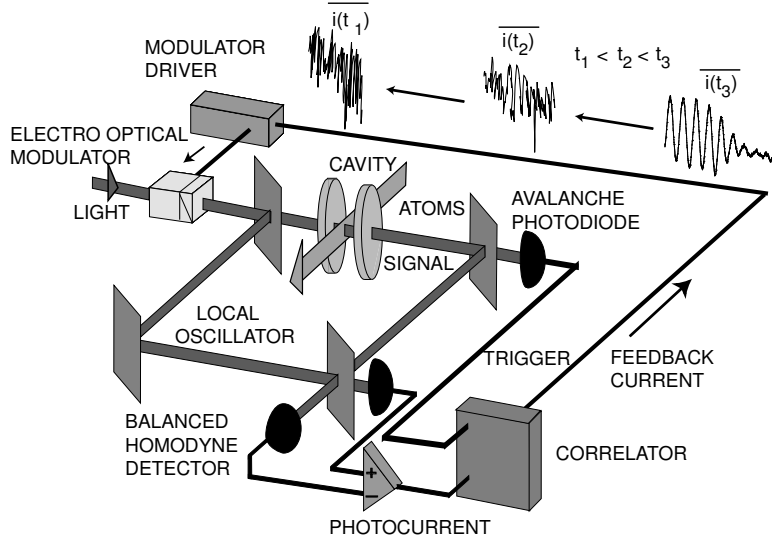


Figure 26. Schematic of the feedback apparatus. The running average is feedback to reduce the contribution of the shot noise component.

which is proportional to the intra-cavity field and contains shot noise ( $\xi(t)$ ). We propose modulating the amplitude of the driving laser with the conditioned BHD photocurrent. This modifies the system Hamiltonian  $H_S$  to include:

$$H_{fb} = \mathcal{G}i(t) (\hat{a} - \hat{a}^\dagger). \quad (68)$$

We improve this feedback by averaging away the shot noise contribution in Eq. (68).

$$H(N, \tau)_{fb} = \frac{\sum_{j=1}^{N_s} \lambda i_c(t_j + \tau)}{N_s} \quad (69)$$

Figure 26 presents a suggestion of how the intensity-field correlator in the experiment of FOSTER, OROZCO, CASTRO-BELTRAN AND CARMICHAEL (2000a) would be modified to apply quantum feedback. Photons arrive at the avalanche photodiode at different times,  $t_1, t_2$  and  $t_3$ . These are well separated to show the reduction in shot noise with consecutive averages.

Figure 27 shows the conditioned field evolution of a single maximally coupled stationary atom in cavity QED without and with the feedback protocol defined by Eq. (68) set to enhance the vacuum Rabi oscillations of the system. The evolution has been maintained well beyond the limits set by  $(\kappa + \gamma_\perp)/2$ . The plot is the result 10,000 averages to reduce the contribution from the shot noise.

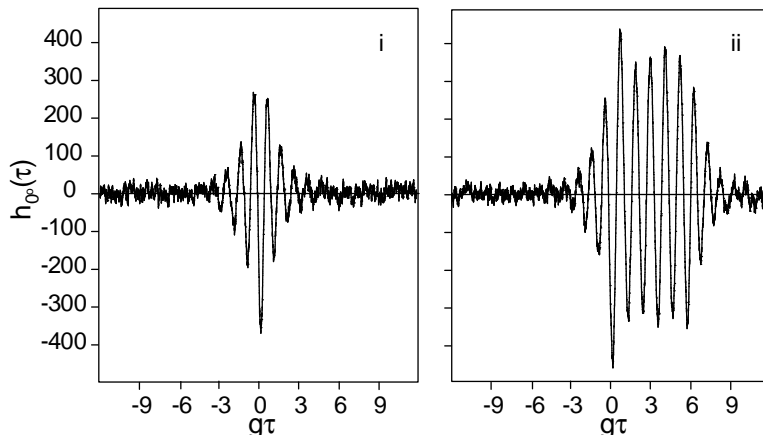


Figure 27. Single atom cavity QED quantum conditioned field evolution: i without feedback, and ii with feedback.  $(g, \kappa, \gamma_{\perp}, \Gamma, \mathcal{G})/2\pi = (38.0, 8.7, 3.0, 100, 3.5)$  MHz.

## 7. Conclusion and Outlook

Future studies may try to map out a full phase space picture of the conditional field as it evolves in time. This would involve sampling the field at various phases and performing some type of tomographic reconstruction to arrive at a quasi-probability distribution (LEONHARDT (1997)).

The conditional homodyne technique may have more general application to studying other sources both classical and non-classical since the information obtained through this intensity-field correlation approach complements and synthesizes that coming from intensity-intensity correlations (particle aspect) and squeezing (wave aspect).

## Acknowledgments

Work supported by NSF and NIST.

## References

- Aharonov, Y., Albert, D. and Vaidman, L. (1988), *Phys. Rev. Lett.* **60**, 1351.
- Aharonov, Y., Albert, D. and Vaidman, L. (1990), *Phys. Rev. A* **41**, 11.
- Bachor, H. A. (1998), *A Guide to Experiments in Quantum Optics*, Wiley-VCH, New York.
- Ban, M. (1996), *J. Mod. Opt.* **43**, 1281.
- Banaszek, K. and Wódkiewicz, K. (1996), *Phys. Rev. Lett.* **76**, 4344.
- Brecha, R. J., Rice, P. R. and Xiao, M. (1999), *Phys. Rev. A* **59**, 2392.
- Brown, R. H. and Twiss, R. Q. (1956), *Nature* **177**, 27.
- Carmichael, H. J. (1987), *J. Opt. Soc. Am. B* **4**, 1588.
- Carmichael, H. J. (1993a), *An Open Systems Approach to Quantum Optics, Lecture Notes in Physics*, Vol. 18, Springer-Verlag, Berlin.

- Carmichael, H. J. (1993b), *Phys. Rev. Lett.* **70**, 2273.
- Carmichael, H. J. (1999), *Statistical Methods in Quantum Optics 1: Master Equations and Fokker-Planck Equations*, Springer-Verlag, Berlin.
- Carmichael, H. J. (2003), *Submitted*.
- Carmichael, H. J. (in press), Quantum fluctuations of light: a modern perspective on wave/particle duality, in A. Thorndike, ed., 'One Hundred Years of the Quantum: from Max Planck to Entanglement', Chicago University Press, Chicago.
- Carmichael, H. J., Brecha, R. J. and Rice, P. R. (1991), *Opt. Commun.* **82**, 73.
- Carmichael, H. J., Brecha, R. J., Raizen, M. G., Kimble, H. J. and Rice, P. J. (1989), *Phys. Rev. A* p. 5516.
- Carmichael, H. J., Castro-Beltran, H. M., Foster, G. T. and Orozco, L. A. (2000), *Phys. Rev. Lett.* **85**, 1855.
- Casimir, H. B. G. (1945), *Rev. Mod. Phys.* **17**, 343.
- Chaturvedi, S. and Drummond, P. D. (1997), *Phys. Rev. A* **55**, 912.
- Clemens, J. P., Rice, P. R., Rungta, P. K. and Brecha, R. J. (2000), *Phys. Rev. A* **62**, 033802.
- Collett, M. J. and Gardiner, C. W. (1984), *Phys. Rev. A* **30**, 1386.
- Collett, M. J. and Gardiner, C. W. (1985), *Phys. Rev. A* **32**, 2887.
- Collett, M. J. and Loudon, R. (1987), *J. Opt. Soc. Am. B* **4**, 1525.
- Crispino, M., Giuseppe, G. D., Martini, F. D., Mataloni, P. & Kanatoulis, H. (2000), *Fortschr. Phys.* **48**, 589.
- Deng, H., Erenso, D., Vyas, R. and Singh, S. (2001), *Phys. Rev. Lett.* **86**, 2770.
- Denisov, A., Castro-Beltran, H. M. and Carmichael, H. J. (2002), *Phys. Rev. Lett.* **88**, 243601.
- Doherty, A. C. and Jacobs, K. (1999), *Phys. Rev. A* **60**, 2700.
- Drummond, P. D. and Kinsler, P. (1995), *Quantum Semiclass. Opt.* **7**, 727.
- Fiurasek, J. (2001), *Phys. Rev. A* **64**, 053817.
- Foster, G. T., Orozco, L. A., Castro-Beltran, H. M. and Carmichael, H. J. (2000a), *Phys. Rev. Lett.* **85**, 3149.
- Foster, G. T., Mielke, S. L. and Orozco, L. A. (2000b), *Phys. Rev. A* **61**, 053821.
- Foster, G. T., Smith, W. P., Reiner, J. E. and Orozco, L. A. (2002), *Phys. Rev. A* **66**, 033807.
- Glauber, R. J. (1963a), *Phys. Rev.* **131**, 2766.
- Glauber, R. J. (1963b), *Phys. Rev. Lett.* **10**, 84.
- Glauber, R. J. (1963c), *Phys. Rev.* **130**, 2529.
- Graham, R. (1971), *Springer Tracts in Modern Physics Vol 66*, 1st edn, Springer-Verlag, Berlin.
- Graham, R. and Haken, H. (1971), *Z. Phys.* **243**, 189.
- Hansen, H., Aichele, T., Hettich, C., Lodahl, P., Lvovsky, A. I., Mlynek, J. and Schiller, S. (2001), *Opt. Lett.* **26**, 1714.
- Jaynes, E. T. and Cummings, F. W. (1963), *Proc. IEEE* **51**, 89.
- Jin, S. and Xiao, M. (1993), *Phys. Rev. A* **48**, 1473.
- Jin, S. and Xiao, M. (1994), *Phys. Rev. A* **49**, 499.
- Kimble, H. J. and Walls, D. F. (1987), *J. Opt. Soc. Am. B* **4**, 1450.
- Kimble, H. J., Dagenais, M. and Mandel, L. (1977), *Phys. Rev. Lett.* **39**, 691.
- Kinsler, P. (1996), *Phys. Rev. A* **53**, 2000.
- Klein, M. J. (1955), *Phys. Rev.* **97**, 1446.
- Leach, J., Strimbu, C. E. and Rice, P. (2003), *Submitted*.
- Leonhardt, U. (1997), *Measuring the Quantum State of Light*, Cambridge University Press, Cambridge.
- Loudon, R. (1980), *Rep. Prog. Phys.* **43**, 913.
- Loudon, R. and Knight, P. L. (1987), 'Squeezed light', *J. Mod. Opt.* **34**, 709.
- Lugiato, L. A. (1984), Theory of optical bistability, in E. Wolf, ed., 'Progress in Optics', Vol. XXI, North-Holland, Amsterdam, pp. 69-216.
- Lutterback, L. G. and Davidovich, L. (1997), *Phys. Rev. Lett.* **78**, 2547.

- Lvovsky, A. I., Hansen, H., Aichele, T., Benson, O., Mlynek, J. and Schiller, S. (2001), *Phys. Rev. Lett.* **87**, 050402.
- Lvovsky, A. I. and Mlynek, J. (2002), *Phys. Rev. Lett.* **88**, 250401.
- Lvovsky, A. I. and Shapiro, J. H. (2002), *Phys. Rev. A* **65**, 033830.
- Mandel, L. and Wolf, E. (1995), *Optical Coherence and Quantum Optics*, Cambridge University Press, New York.
- Milburn, G. and Walls, D. F. (1981), *Opt. Commun.* **39**, 401.
- Onsager, L. (1931), *Phys. Rev.* **37**, 405.
- Paul, H. (1982), *Rev. Mod. Phys.* **54**, 1061.
- Pope, D. T., Drummond, P. D. and Munro, W. J. (2000), *Phys. Rev. A* **60**, 052108.
- Reiner, J. E., Smith, W. P., Orozco, L. A., Carmichael, H. J. and Rice, P. R. (2001), *J. Opt. Soc. Am. B* **18**, 1911.
- Resch, K. J., Lundeen, J. S. and Steinberg, A. M. (2002a), *Phys. Rev. Lett.* **88**, 113601.
- Resch, K. J., Lundeen, J. S. and Steinberg, A. M. (2002b), *Phys. Rev. Lett.* **89**, 037904.
- Rice, P. R. and Carmichael, H. J. (1988), *J. Opt. Soc. Am. B* **5**, 1661.
- Siddiqui, S., Erenso D., Vyas R., and Singh S.(2003),*Phys. Rev. A* **67**, 06380855.
- Slusher, R. E., Hollberg, L. W., Mertz, J. C., Yurke, B. and Valley, J. F. (1985), *Phys. Rev. Lett.* **55**, 2409.
- Smith, W. P., Reiner J. E., Orozco L. A., Kuhr S. and Wiseman H. M. (2002), *Phys. Rev. Lett.* **89**, 133601.
- Strimbu, C. E. and Rice, P. R. (2003), *Submitted*.
- Tolman, R. C. (1938), *The Principles of Statistical Mechanics*, Oxford University Press, London.
- Tombesi, P. and Vitali, D. (1995), *Phys. Rev. A* **51**, 4913.
- Tomita, K. and Tomita, H. (1973), *Phys. Lett. A* **46**, 265.
- Tomita, K. and Tomita, H. (1974), *Prog. Th. Phys.* **51**, 1731.
- Vogel, W. (1991), *Phys. Rev. Lett.* **67**, 2450.
- Vyas, R. and Singh, S. (2000), *Phys. Rev. A* **62**, 0338033.
- Wallentowitz, S. and Vogel, W. (1996), *Phys. Rev. A* **53**, 4528.
- Walls, D. F. (1979), *Nature* **280**, 451.
- Wiseman, H. M. (1994), *Phys. Rev. A* **49**, 2133.
- Wang, J. and Wiseman, H. M. (2001), *Phys. Rev. A* **64**, 063810.
- Wiseman, H. M. (2002), *Phys. Rev. A* **65**, 032111.
- Yuen, H. P. and Chan, V. W. (1983a), *Opt. Lett.* **8**, 177.
- Yuen, H. P. and Chan, V. W. (1983b), 'Errata', *Opt. Lett.* **8**, 345.
- Yurke, B. and Stoler, D. (1987), *Phys. Rev. A* **36**, 1955.